EUROPEAN ORGANIZATION FOR NUCLEAR RESEARCH

Azimuthal anisotropy of charged jet production in $\sqrt{s_{\mathrm{NN}}}$ = 2.76 TeV Pb–Pb collisions

ALICE Collaboration[*]

Abstract

We present measurements of the azimuthal dependence of charged jet production in central and semi-central $\sqrt{s_{\mathrm{NN}}}$ = 2.76 TeV Pb–Pb collisions with respect to the second harmonic event plane, quantified as $v_2^{\mathrm{ch\,jet}}$. Jet finding is performed employing the anti-k_{T} algorithm with a resolution parameter $R = 0.2$ using charged tracks from the ALICE tracking system. The contribution of the azimuthal anisotropy of the underlying event is taken into account event-by-event. The remaining (statistical) region-to-region fluctuations are removed on an ensemble basis by unfolding the jet spectra for different event plane orientations independently. Significant non-zero $v_2^{\mathrm{ch\,jet}}$ is observed in semi-central collisions (30–50% centrality) for $20 < p_{\mathrm{T}}^{\mathrm{ch\,jet}} < 90$ GeV/c. The azimuthal dependence of the charged jet production is similar to the dependence observed for jets comprising both charged and neutral fragments, and compatible with measurements of the v_2 of single charged particles at high p_{T}. Good agreement between the data and predictions from JEWEL, an event generator simulating parton shower evolution in the presence of a dense QCD medium, is found in semi-central collisions.

[*]See Appendix A for the list of collaboration members

arXiv:1509.07334v1 [nucl-ex] 24 Sep 2015

1 Introduction

The aim of the heavy-ion program at the LHC is to study strongly interacting matter in ultra-relativistic nuclear collisions where the formation of a quark-gluon plasma (QGP), a deconfined state of quarks and gluons, is expected [1]. Hard partons that propagate through the collision medium lose energy via (multiple) scattering and gluon radiation [2, 3]. Jet measurements are used to experimentally explore parton energy loss in the hot and dense medium. Studies at the LHC and RHIC have shown that jet and high-p_T single particle production in heavy-ion collisions are suppressed with respect to the expected production in a superposition of independent pp collisions [4–13]. This observation is consistent with energy loss, which is further supported by measurements of dijet energy asymmetry and di-hadron angular correlations [14–16].

In non-central Pb–Pb collisions, the initial overlap region of the colliding nuclei projected into the plane perpendicular to the beam direction has an approximately elliptic shape. Jets emitted along the minor axis of the ellipse (defined as the *in-plane* direction) on average traverse less medium - and are therefore expected to lose less energy - than jets that are emitted along the major axis of the ellipse (the *out-of-plane* direction). The dependence of jet production on the angle relative to the second-harmonic symmetry plane Ψ_2 (the symmetry plane angles Ψ_n define the orientations of the symmetry axes of the initial nucleon distribution of the collision) can be used to probe the path-length dependence of jet energy loss. This dependence is quantified by the parameter $v_2^{\mathrm{ch\,jet}}$, the coefficient of the second term in a Fourier expansion of the azimuthal distribution of jets relative to symmetry planes Ψ_n,

$$\frac{\mathrm{d}N}{\mathrm{d}\left(\varphi_{\mathrm{jet}} - \Psi_n\right)} \propto 1 + \sum_{n=1}^{\infty} 2v_n^{\mathrm{jet}} \cos\left[n\left(\varphi_{\mathrm{jet}} - \Psi_n\right)\right], \tag{1}$$

where φ_{jet} denotes the azimuthal angle of the jet.

In central collisions, the average distance that a jet propagates through the medium is approximately equal in the in-plane and out-of-plane directions, therefore a small $v_2^{\mathrm{ch\,jet}}$ is expected. In semi-central collisions the average in-medium distance is shorter, while the relative difference between the average distances in-plane and out-of-plane is larger, hence a non-zero $v_2^{\mathrm{ch\,jet}}$ is expected. Fluctuations in the initial distribution of nucleons within the overlap region can lead to additional contributions to $v_2^{\mathrm{ch\,jet}}$ and higher harmonic coefficients in the Fourier decomposition.

The path-length dependence of parton energy loss is of particular interest because it is sensitive to the underlying energy-loss mechanism. For collisional (elastic) energy loss, the amount of lost energy depends linearly on path length, while for radiative (inelastic) energy loss, the dependence is quadratic due to interference effects [17, 18]. Some strong-interaction models based on the AdS/CFT correspondence suggest an even stronger path-length dependence [19, 20]. Earlier studies of the v_2 of high-p_T single particles have already tested the path-length dependence of energy loss [21–25]. Comparisons of these results to theoretical calculations have shown that the v_2 is sensitive to several aspects of the medium evolution, including the effects of longitudinal and transverse expansion and the life time of the system until freeze-out [26]. It is therefore important to measure multiple observables that are sensitive to the path-length dependence of energy loss, such as recoil yields of charged particles and jets [11, 27, 28]. Jets are expected to better represent the original parton kinematics and provide more detailed information on energy loss. Theoretical predictions from JEWEL, which couples parton shower evolution to the presence of a QCD medium with a density derived from Glauber simulations [29, 30], have shown that a finite v_2^{jet} is expected for non-central collisions at the LHC. Similar results have been found in v_2^{jet} studies in heavy-ion collisions generated by the AMPT model [31, 32].

The largest experimental challenge in jet analyses in heavy-ion collisions is the separation of the jet signal from the background of mostly low-p_T particles from the underlying event and from unrelated scatterings that take place in the collision. In this analysis, the jet energy is corrected on a jet-by-

jet basis using an estimate of the background energy density which takes into account the azimuthal anisotropy of the background event-by-event, as will be described in Sections 2.1 and 2.2. The in-plane and out-of-plane jet spectra are unfolded independently to take into account detector effects and remaining azimuthally-dependent fluctuations in the underlying event energy density (Sec. 2.3). The coefficient $v_2^{\mathrm{ch\ jet}}$ is calculated from the difference of jet yields in the in-plane and out-of-plane directions and corrected for the finite event plane resolution, as described in Sec. 2.4. An overview of systematic uncertainties is given in Sec. 2.5. The results are presented in Sec. 3, while in Sec. 3.1 comparisons to theoretical predictions and other v_2 measurements are discussed.

2   Experimental setup and data analysis

ALICE is a dedicated heavy-ion experiment at the LHC at CERN. A full overview of the detector layout and performance can be found in [33, 34]. The central barrel detector system, covering full azimuth, is positioned in a solenoidal magnet with a field strength of 0.5 T. It comprises the Inner Tracking System (ITS) built from six layers of silicon detectors (the Silicon Pixel, Drift, and Strip Detectors: SPD, SDD and SSD) and a Time Projection Chamber (TPC). The two inner layers of the ITS, which comprise the SPD, are located at 3.9 and 7.2 cm radial distance from the beam axis.

The data presented in this paper were recorded in the Pb–Pb data taking periods in 2010 and 2011 at $\sqrt{s_{\mathrm{NN}}}$ = 2.76 TeV, using a minimium-bias trigger (2010) or an online centrality trigger for hadronic interactions (2011), which requires a minimum multiplicity in both the V0A and V0C detectors (discs of segmented scintillators covering full azimuth and $2.8 < \eta < 5.1$ and $-3.7 < \eta < -1.7$, respectively). The V0 detectors are used to determine event centrality based on the energy deposition in the scintillator tiles [35] and the event plane orientation, see Sec. 2.1. Centrality is expressed as percentiles of the total hadronic cross section, with 0–5% referring to the most central (largest multiplicity) events. Time information from the V0 detectors is used to reject beam-gas interactions from the event sample and the remaining contribution of such interactions is negligible. Only events with a primary vertex position within ± 10 cm along the beam direction from the nominal interaction point were used in the analysis. A total of 6.8×10^6 events with 0–5% centrality and 8.6×10^6 events with 30–50% centrality, corresponding to integrated luminosities of 18 and 5.6 $\mu\mathrm{b}^{-1}$, respectively, are used in this analysis.

Charged particle tracks in this analysis are measured by the ITS and TPC and are selected in a pseudora-pidity range $|\eta| < 0.9$ with transverse momenta $0.15 < p_{\mathrm{T}} < 100$ GeV/c. To ensure a good momentum resolution, tracks were required to have at least three hits per track in the ITS. Since the SPD acceptance is non-uniform in azimuth for the data sample used in this analysis, two classes of tracks are used. The first class requires at least three hits per track in the ITS, with at least one hit per track in the SPD. The second class contains tracks without hits in the SPD, in which case the primary interaction vertex is used as an additional constraint for the momentum determination. For each track, the expected number of TPC space points is calculated based on its trajectory; tracks are accepted if they have at least 80% of the expected TPC space-points, with a minimum of 70 TPC points.

2.1   Event plane determination

The coefficient $v_2^{\mathrm{ch\ jet}}$ quantifies azimuthal anisotropy with respect to Ψ_2. The azimuthal anisotropy of the underlying event ('background flow') is also described by a Fourier series with harmonics $v_n = \langle \cos(n[\varphi - \Psi_n]) \rangle$ [36, 37] where φ denotes the track azimuthal angle. However, since the initial distribution of nucleons is not accessible experimentally, the *event plane angles* $\Psi_{\mathrm{EP},\,n}$, *i.e.* the axes of symmetry of the density of outgoing particles in the transverse plane, are used in place of Ψ_n when measuring $v_2^{\mathrm{ch\ jet}}$ and v_n.

The event plane angles $\Psi_{\mathrm{EP},\,2}$ and $\Psi_{\mathrm{EP},\,3}$ in this study, corresponding to the two dominant Fourier harmonics, are reconstructed using the V0 detectors. Each V0 array consists of four rings in the radial

direction, with each ring comprising eight cells with the same azimuthal size. The calibrated amplitude of the signal in each cell, proportional to the multiplicity incident on the cell, is used as a weight w_{cell} in the construction of the flow vectors Q_n [38]

$$Q_n = \sum_{\text{cells}} w_{\text{cell}} \exp\left(i\, n\, \varphi_{\text{cell}}\right). \tag{2}$$

In order to account for a non-uniform detector response which can generate a bias in the $\Psi_{\text{EP},\, n}$ azimuthal distribution, the components of the Q_n-vectors are adjusted using a re-centering procedure [39, 40]. The V0A and V0C detectors cover different η regions in which multiplicity N and background flow v_n may differ. The total V0 Q-vector is therefore constructed using weights χ_n [38] that are approximately proportional to the event plane resolution in each detector,

$$Q_{n,\text{V0}} = \chi^2_{n,\text{V0A}} Q_{n,\text{V0A}} + \chi^2_{n,\text{V0C}} Q_{n,\text{V0C}}, \tag{3}$$

to achieve the optimal combined event plane resolution. The event planes are reconstructed from the real and imaginary parts of Q_n as

$$\Psi_{\text{EP},\, n} = \arctan\left(\frac{\Im\left[Q_n\right]}{\Re\left[Q_n\right]}\right) / n. \tag{4}$$

The $v_2^{\text{ch jet}}$ itself is measured with respect to the second harmonic event plane angle. It is corrected for the finite precision with which the true symmetry plane is measured in the V0 system by applying an event plane resolution correction, see Sec. 2.4.

2.2 Jet reconstruction in the presence of background flow

Jet finding is performed using the FastJet [41, 42] implementation of the infrared and collinear safe k_{T} and anti-k_{T} sequential recombination algorithms, with resolution parameter $R = 0.2$. The resolution parameter determines the characteristic maximum distance of constituent tracks to the jet axis in the $\eta - \varphi$ plane.

In heavy-ion collisions, a large combinatorial background is present from particles that are not related to the hard scattering that produced a given jet. This background is subtracted from each jet on an event-by-event basis. The anti-k_{T} algorithm is used to find *signal jets*. A fiducial cut of $|\eta_{\text{jet}}| < 0.7$ is applied on the signal jets to ensure that all jets are fully contained within the ITS and TPC acceptances and edge effects are avoided. The contribution of *combinatorial* (or 'fake') jets (clustered underlying event energy) to the measured jet spectrum is reduced by requiring that reconstructed jets contain at least one charged particle with $p_{\text{T}} > 3$ GeV/c and have an area of at least $0.56\,\pi R^2$. These selection criteria leave the hard part of the jet spectrum unaltered while significantly reducing the number of combinatorial jets which stabilizes the unfolding procedure [4, 5, 43].

The k_{T}-algorithm is used to estimate the average energy density of the underlying event, $\langle \rho_{\text{ch}} \rangle$, on an event-by-event basis. The quantity $\langle \rho_{\text{ch}} \rangle$ is the median of the distribution of $p_{\text{T,chjet}}^{\text{raw}}/A$ (the ratio of transverse momentum to jet area) of reconstructed k_{T}-jets, excluding the leading two jets from the sample as proposed in [44] and implemented in earlier ALICE jet studies [4, 5, 43]. The jet area A is determined by embedding a fixed number of near zero-momentum *ghost particles* per event prior to jet finding; the number of ghost particles in each reconstructed jet then gives a direct measure of the jet area. A ghost density of 200 particles per unit area is used, so that approximately 25 ghost particles are clustered into a jet with a radius of 0.2.

In each event, the anisotropy of the underlying event is modeled using the dominant [45] flow harmonics v_2 and v_3,

$$\rho_{\text{ch}}(\varphi) = \rho_0 \left(1 + 2\{v_2 \cos\left[2\left(\varphi - \Psi_{\text{EP},\, 2}\right)\right] + v_3 \cos\left[3\left(\varphi - \Psi_{\text{EP},\, 3}\right)\right]\}\right). \tag{5}$$
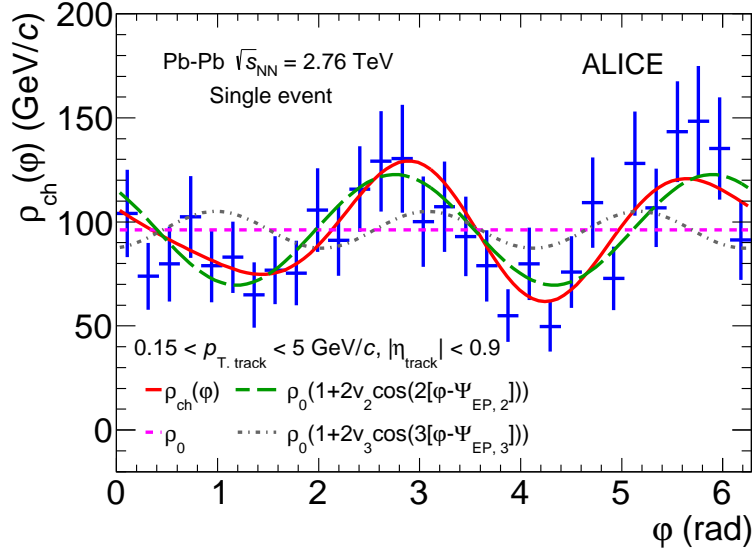
4

Fig. 1: Transverse momentum density of charged tracks as a function of azimuthal angle for a single event from the most central 0-5% event class. Data points (blue) are given with statistical uncertainties only. The red curve is the fit of Eq. 5 to the distribution, the green and gray curves, obtained from the fit of Eq. 5 as well, show the independent contributions of v_2 and v_3 to $\rho_{ch}(\varphi)$. The dashed magenta line is the normalization constant ρ_0.

Here, $\rho_{ch}(\varphi)$ is the azimuthal distribution of summed track p_T for tracks with $0.15 < p_T < 5$ GeV/c and $|\eta_{track}| < 0.9$. The parameters ρ_0 and v_n are determined event-by-event from a fit of the right side of Eq. 5 to the data. The event plane angles $\Psi_{EP, n}$ are not fitted, but fixed to the V0 event plane angles. A single event example of this procedure is illustrated in Fig. 1, where the data points represent the transverse momentum density distribution in a single event, the red curve represents the full functional description of $\rho_{ch}(\varphi)$ (Eq. 5), the green and gray curves give the contributions of the separate harmonics v_2 and v_3, and the dashed magenta line is the normalization constant ρ_0. To reduce the bias of hard jets in the estimates of v_n in Eq. 5 while retaining azimuthal uniformity, the leading jet in each event is removed by rejecting all tracks for which $|\eta_{jet} - \eta_{track}| < R$. The η separation between the tracks and the V0 detectors also removes short range correlations between the event planes and tracks.

The number of bins to which Eq. 5 is fitted is set on an event-by-event basis to the square root of the number of tracks. The fit maximizes the estimated likelihood [46], which is based on a Poisson distribution for the bin content. Since the bin contents are not pure counts, but weighted by p_T, the statistical uncertainties on each bin σ_i are estimated as the sum of the squares of the p_T of the individual particles: $\sigma_i = \sigma(\sum p_T) = \sqrt{\sum p_T^2}$. A scaled Poisson distribution $w_i P(x_i | \mu_i / w_i)$ is used as the probability distribution for the data points in the likelihood calculation, with a scale factor $w_i = \sigma_i^2 / y_i$ where y_i is the bin content and μ_i / w_i is the expected signal from the fit function. The compatibility of each fit with the data is tested by calculating the χ^2 and evaluating the probability of finding a test statistic at least as large as the observed one in the χ^2 distribution. When this probability is less than 0.01, the average event background density $\langle \rho_{ch} \rangle$ is used instead of $\rho_{ch}(\varphi)$; this occurs in 3% (most central) to 7% (semi-central) of events. The acceptance criterion is varied in the systematic studies; the sensitivity to it is small.

The corrected transverse momentum p_T^{chjet} of a jet of area A is calculated from the measured raw jet momentum, $p_{T,chjet}^{raw}$, as

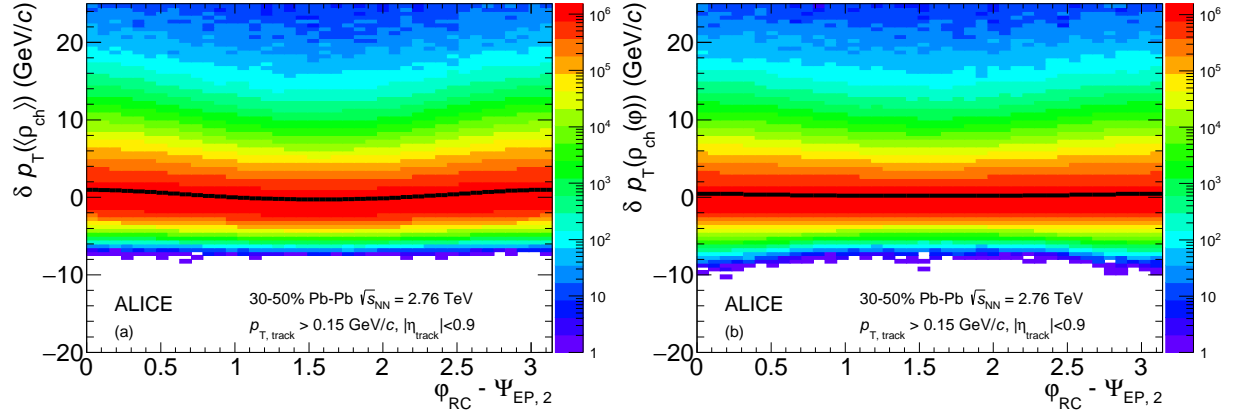$$p_T^{chjet} = p_{T,chjet}^{raw} - \rho_{ch\ local} A \tag{6}$$

5

Fig. 2: The δp_T distribution (Eq. 8) from the random cone (RC) procedure as function of cone azimuthal angle φ_{RC} relative to the event plane. In panel (a) the azimuthally-averaged background $\langle \rho_{ch} \rangle$ has been subtracted; in panel (b) the azimuthally dependent $\rho_{ch}(\varphi)$ from an event-by-event fit of the p_T-density with Eq. 5. The solid black line represents the mean of the δp_T distribution.

where $\rho_{ch\,local}$ is obtained from integration of $\rho_{ch}(\varphi)$ around $\varphi_{jet} \pm R$

$$\rho_{ch\,local} = \frac{\langle \rho_{ch} \rangle}{2R\rho_0} \int_{\varphi-R}^{\varphi+R} \rho_{ch}(\varphi)d\varphi. \tag{7}$$

The pre-factor of the integral, $\frac{\langle \rho_{ch} \rangle}{2R\rho_0}$, is chosen such that integration over the full azimuth yields the average energy density $\langle \rho_{ch} \rangle$. The validity of Eq. 5 as a description of the contribution of background flow to the underlying event energy is tested by placing cones of radius $R = 0.2$ at random positions (excluding the location of the leading jet) in the η–ϕ plane and subtracting the expected summed transverse momentum in a cone from the measured transverse momentum in the cone,

$$\delta p_T = \sum p_T^{tracks} - \rho \pi R^2. \tag{8}$$

Here, ρ is the expected transverse momentum density. This procedure is repeated multiple times per event, until the full phase space is covered, to obtain a distribution of δp_T values. The δp_T distribution as a function of the cone azimuthal angle φ_{RC} relative to the event plane $\Psi_{EP,\,2}$ is shown in Fig. 2. In panel (a) $\langle \rho_{ch} \rangle$ has been used for the estimation of the underlying event summed p_T and in panel (b) $\rho_{ch}(\varphi)$. Incorporating azimuthal dependence into the underlying event description leads to a sizable reduction in the cosine modulation of the δp_T distribution.

The effectiveness of the subtraction of background flow is quantified by comparing the expected and measured widths of the δp_T distribution in the *absence* of background flow, $\sigma(\delta p_T^{v_n=0})$, (see Fig. 2b) to the expected and measured widths of the δp_T distribution in the *presence* of background flow, $\sigma(\delta p_T^{v_n})$ (Fig. 2a). Assuming independent particle emission and Poissonian statistics, the expected width of the δp_T distribution in the absence of background flow ($v_n = 0$) is given by [43]

$$\sigma(\delta p_T^{v_n=0}) = \sqrt{N_A \sigma^2(p_T) + N_A \langle p_T \rangle^2} \tag{9}$$

where N_A is the average expected number of tracks within a cone, $\langle p_T \rangle$ the mean p_T of a single particle spectrum and $\sigma(p_T)$ the standard deviation of this spectrum. This expectation can be extended to include contributions from background flow by introducing non-Poissonian density fluctuations (the background flow harmonics v_n) [43], as

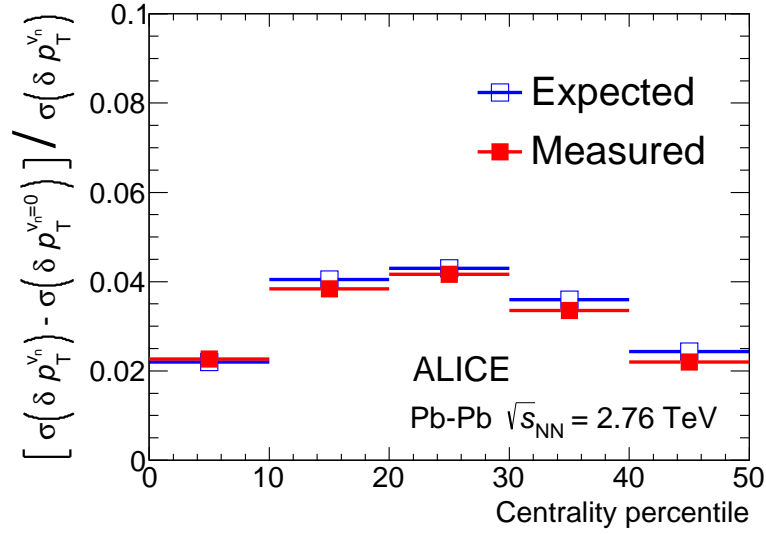$$\sigma(\delta p_T^{v_n}) = \sqrt{N_A \sigma^2(p_T) + (N_A + 2N_A^2(v_2^2 + v_3^2))\langle p_T \rangle^2}. \tag{10}$$

6

Fig. 3: Centrality dependence of the measured and expected relative change in the δp_T distribution width from using the azimuthally dependent $\rho_{\text{ch local}}$ instead of the median $\langle \rho_{\text{ch}} \rangle$. The blue points give the expected reduction from simple assumptions about the behavior of charged particle spectra and flow harmonics v_n (following Eq. 9 and 10). The red points use the measured widths from δp_T distributions directly. Statistical uncertainties are smaller than the marker size.

The measured widths are obtained from the δp_T distributions directly; the distributions are constructed using as the energy density ρ in Eq. 8 either $\langle \rho_{\text{ch}} \rangle$ to obtain $\sigma(\delta p_T^{v_n})$ or $\rho_{\text{ch local}}$ for $\sigma(\delta p_T^{v_n=0})$.

Figure 3 shows the expected and measured relative change in the width of the δp_T distribution, quantified as $(\sigma(\delta p_T^{v_n}) - \sigma(\delta p_T^{v_n=0}))/\sigma(\delta p_T^{v_n})$, as function of collision centrality. The blue points give the expected reduction from Eqs 9 and 10. The red points use the measured widths from δp_T distributions. The expected change is in good quantitative agreement with the measured change over the entire centrality range, indicating that the width of the δp_T distributions can be understood in terms of a simple independent particle emission model with background flow contributions.

The background subtraction, unfolding, correction for the reaction plane resolution as described in Sections 2.3 and 2.4 were also validated using events consisting of PYTHIA jets embedded in heavy-ion background events and toy model events. In the first study, full PYTHIA pp events were combined with reconstructed Pb–Pb collisions to create events with a controlled signal and background. The signal jets from PYTHIA have no preferred orientation, $v_2^{\text{ch jet}} = 0$, while the heavy-ion events have a non-zero v_2 of the soft particles. Jets found in the events were matched to the embedded PYTHIA jets and the analysis was carried out with matched jets only. After unfolding, the $v_2^{\text{ch jet}}$ was compatible with 0, as expected. The other study was based on events generated using a simple thermal model for soft particle production and a distribution of high-p_T particles that resembles the jet spectrum, as suggested in [47]. A non-zero $v_2 = 0.07$ was introduced for momenta $p_T < 5$ GeV/c to model the background flow and two variations at large $p_T > 30$ GeV/c: $v_2 = 0$ or $v_2 = 0.05$. In both cases, the input flow values were correctly reconstructed by the analysis.

2.3 Unfolding

After the subtraction procedure presented in the previous section, the measured jet spectrum is unfolded [48, 49] to correct for detector effects and fluctuations in the underlying event energy density. Mathe-

matically, the unfolded jet spectrum can be derived from the measured spectrum by solving

$$M(p_{\mathrm{T,chjet}}^{\mathrm{rec}}) = \int G(p_{\mathrm{T,chjet}}^{\mathrm{rec}}, p_{\mathrm{T,chjet}}^{\mathrm{gen}}) T(p_{\mathrm{T,chjet}}^{\mathrm{gen}}) \varepsilon(p_{\mathrm{T,chjet}}^{\mathrm{gen}}) \mathrm{d} p_{\mathrm{T,chjet}}^{\mathrm{gen}} \tag{11}$$

for $T(p_{\mathrm{T,chjet}}^{\mathrm{gen}})$, the unfolded true jet spectrum, where $M(p_{\mathrm{T,chjet}}^{\mathrm{rec}})$ is the measured jet spectrum, $G(p_{\mathrm{T,chjet}}^{\mathrm{rec}}, p_{\mathrm{T,chjet}}^{\mathrm{gen}})$ is a functional description (*response function*) of distortions due to background fluctuations and detector response, and $\varepsilon(p_{\mathrm{T,chjet}}^{\mathrm{gen}})$ is the jet finding efficiency. The coefficient $v_2^{\mathrm{ch\,jet}}$ is not affected by the efficiency, hence $\varepsilon(p_{\mathrm{T,chjet}}^{\mathrm{gen}})$ will be omitted from here on. Since the measured jet spectrum is binned, Eq. 11 is discretized by replacing the integral by a matrix multiplication

$$\mathbf{M_m} = \mathbf{G_{m,t}} \cdot \mathbf{T'_t} \tag{12}$$

where $\mathbf{T'_t}$ is the solution of the discretized equation (the prime indicates that $\mathbf{T'_t}$ is not corrected for jet-finding efficiency). The combined response matrix $\mathbf{G_{m,t}}$ is the product of the response matrices from detector effects and energy density fluctuations, the latter of which are constructed independently for the in-plane and out-of-plane spectra by embedding random cones at specific relative azimuth with respect to the event plane (see the text below Eq. 13 for the definition of the intervals).

The detector response matrix is obtained by matching pp jets generated by PYTHIA [50] to the *same* jets after transport through the detector by GEANT3 [51], where the detector conditions are tuned to those of the data-taking periods. Matching is based on the shortest distance in the η–φ plane between transported (detector level) and pure PYTHIA (particle level) jets and is bijective, meaning that there is a one-to-one correspondence between detector and particle level jets. The response matrix for background fluctuations is constructed from the δp_{T} distributions, which, when normalized, are probability distributions for the change of the jet energy caused by background fluctuations.

Solving Eq. 12 requires inversion of $\mathbf{G_{m,t}}$ and generally leads to non-physical results which oscillate wildly due to the statistical fluctuations of the measured jet yield. The unfolded solution therefore needs to be regularized. In general this is done by introducing a penalty term for large local curvatures associated with oscillations. Various algorithms for regularized unfolding exist; the unfolding method based on the Singular Value Decomposition (SVD unfolding) [52] is used in this study. A comparison to the unfolded solution from χ^2 minimization [53] is used in the systematic studies.

The measured jet spectrum is taken as input for the unfolding routine in the range $30 < p_{\mathrm{T}}^{\mathrm{chjet}} < 105$ GeV/c for 0–5% collision centrality and $15 < p_{\mathrm{T}}^{\mathrm{chjet}} < 90$ GeV/c for 30–50% collision centrality. The lower bound corresponds to five times the width of the δp_{T} distribution, the upper bound is the edge of the last measured bin which contains at least 10 counts. This configuration was found to lead to reliable unfolded solutions in Monte Carlo studies [4, 47]. The unfolded jet spectrum starts at 0 GeV/c to allow for feed-in of true jets with low $p_{\mathrm{T}}^{\mathrm{chjet}}$. In addition, combinatorial jets which are not rejected by the jet area and leading charged particle requirements are migrated to momenta lower than the minimum measured $p_{\mathrm{T}}^{\mathrm{chjet}}$. The unfolded solution ranges up to 200 GeV/c (0–5%) and 170 GeV/c (30–50%) to allow for migration of jets to a $p_{\mathrm{T}}^{\mathrm{chjet}}$ higher than the maximum measured momentum. As the data points of the unfolded solution are strongly correlated for $p_{\mathrm{T}}^{\mathrm{chjet}}$ outside the experimentally measured interval, $v_2^{\mathrm{ch\,jet}}$ will be reported only within the limits of the measured jet spectra.

2.4 Evaluation of $v_2^{\mathrm{ch\,jet}}$

The coefficient $v_2^{\mathrm{ch\,jet}}$ is calculated from the difference between the unfolded p_{T}-differential jet yields in-plane (N_{in}) and out-of-plane (N_{out}) with respect to the second harmonic event plane, corrected for event plane resolution,

$$v_2^{\mathrm{ch\,jet}}(p_{\mathrm{T}}^{\mathrm{chjet}}) = \frac{\pi}{4} \frac{1}{\mathscr{R}_2} \frac{N_{\mathrm{in}}(p_{\mathrm{T}}^{\mathrm{chjet}}) - N_{\mathrm{out}}(p_{\mathrm{T}}^{\mathrm{chjet}})}{N_{\mathrm{in}}(p_{\mathrm{T}}^{\mathrm{chjet}}) + N_{\mathrm{out}}(p_{\mathrm{T}}^{\mathrm{chjet}})}. \tag{13}$$

Eq. 13 is derived by integrating Eq. 1 for $n = 2$, over intervals $\left[-\frac{\pi}{4}, \frac{\pi}{4}\right]$ and $\left[\frac{3\pi}{4}, \frac{5\pi}{4}\right]$ for N_{in} and $\left[\frac{\pi}{4}, \frac{3\pi}{4}\right]$ and $\left[\frac{5\pi}{4}, \frac{7\pi}{4}\right]$ for N_{out}, substituting $\Psi_{\text{EP, 2}}$ for Ψ_2. Eq. 13 is sensitive to correlations between even-order harmonics v_{2n} and $\Psi_{\text{EP, 2}}$. As a result of the integration limits however, the first harmonic of the Fourier expansion that can contribute to the observed $v_2^{\text{ch jet}}$ is $v_6^{\text{ch jet}}$. The V0 event plane resolution $\mathcal{R}_2$ is introduced to account for the finite precision with which the true symmetry plane Ψ_2 is measured in the V0 system and is defined as

$$\mathcal{R}_2 = \left\langle \cos\left[2\left(\Psi_{\text{EP, 2}}^{\text{V0}} - \Psi_2\right)\right]\right\rangle. \tag{14}$$

Measuring event planes in multiple η regions (*sub-events*) allows for the evaluation of the resolution directly from data [54, 55]. Using the full V0 detector and negative and positive η sides of the TPC as sub-events, the resolution in Eq. 13 is evaluated as

$$\mathcal{R}_2 = \left(\frac{\left\langle \cos\left[2\left(\Psi_{\text{EP, 2}}^{\text{V0}} - \Psi_{\text{EP, 2}}^{\text{TPC}, \eta > 0}\right)\right]\right\rangle \left\langle \cos\left[2\left(\Psi_{\text{EP, 2}}^{\text{V0}} - \Psi_{\text{EP, 2}}^{\text{TPC}, \eta < 0}\right)\right]\right\rangle}{\left\langle \cos\left[2\left(\Psi_{\text{EP, 2}}^{\text{TPC}, \eta > 0} - \Psi_{\text{EP, 2}}^{\text{TPC}, \eta < 0}\right)\right]\right\rangle}\right)^{1/2}. \tag{15}$$

The event plane resolution $\mathcal{R}_2$ is found to be 0.47 in 0–5% centrality and 0.75 in 30–50% centrality with negligible uncertainties. The $\Psi_{\text{EP, 2}}$ angles in the TPC are obtained following the procedure of Eq. 4 on tracks with $0.15 < p_{\text{T}} < 4$ GeV/c, using unit track weights in the construction of the flow vectors Q_2 (see Eq. 2).

Using the V0 detectors for the reconstruction of the event plane guarantees that the jet axis and event plane information are separated in pseudorapidity by $|\Delta\eta| > 1$ and thus removes autocorrelation biases between the signal jets and event plane orientation. The possible non-flow correlation between the event plane angle and jets due to di-jets with one jet at mid-rapidity and one jet in the V0 acceptance was studied using the PYTHIA event generator. The rate of such di-jet configurations was found to be negligible (less than 1 per mille of the total di-jet rate at mid-rapidity) for $p_{\text{T}}^{\text{chjet}} > 20$ GeV. Possible effects from back-to-back jet pairs with a jet in each of the V0 detectors are even smaller.

2.5 Systematic uncertainties

Systematic uncertainties on $v_2^{\text{ch jet}}$ are grouped into two categories, *shape* and *correlated*, based on their point-to-point correlation. Shape uncertainties are anti-correlated between parts of the unfolded spectrum: when the yield in part of the spectrum increases, it decreases elsewhere and vice versa. Correlated uncertainties are correlated point-to-point. Both types of uncertainties however have contributions which lead to correlated changes of N_{in} and N_{out}.

Correlated uncertainties are estimated for the in-plane and out-of-plane jet spectra independently. The dominant correlated uncertainty ($\lesssim 10\%$) arises from tracking and is estimated by constructing a detector response matrix with a tracking efficiency reduced by 4% (motivated by studies [4] comparing reconstrcucted tracks to simulations of HIJING [56] events). The observed difference between the nominal and modified unfolded solution is taken as a symmetric uncertainty to allow for an over- and underestimation of the tracking efficiency. The sensitivity of the unfolded result to combinatorial jets is tested by changing the lower range of the unfolded solution from 0 to 5 GeV/c, which leads to an overall (correlated) increase of the unfolded jet yield. Both correlated uncertainties are added in quadrature and propagated to $v_2^{\text{ch jet}}$ assuming that variations are strongly correlated between the in-plane and out-of-plane jet spectra, while still allowing for effects from azimuthally dependent variations in track occupancy, by setting the sample correlation coefficient $\rho \equiv \sigma_{i,j}/(\sigma_i \sigma_j)$ to 0.75.

Shape uncertainties fall into three categories: assumptions in the unfolding procedure, feed-in of combinatorial jets, and the sensitivity of the unfolded solution to the shape of the underlying event energy distribution. The dominant contribution to the unfolding uncertainty is related to the regularization of the unfolded solution. The SVD algorithm [52] regularizes the unfolding by omitting components of the

		Uncertainty on $v_2^{\text{ch jet}}$					
	p_T^{chjet} (GeV/c)	30–40	60–70	80–90	30–40	60–70	80–90
	Centrality (%)	0–5			30–50		
Shape	Unfolding	0.017	0.012	0.016	0.016	0.011	0.015
	p_T^{chjet}-measured	0.013	$\ll$ stat	$\ll$ stat	0.024	$\ll$ stat	$\ll$ stat
	$\rho_{\text{ch}}(\varphi)$fit	0.015	$\ll$ stat	0.016	$\ll$ stat	$\ll$ stat	$\ll$ stat
Total		0.027	0.012	0.023	0.029	0.011	0.015
Correlated	Tracking	0.009	0.009	0.009	0.007	0.007	0.007
	p_T^{chjet}-unfolded	$\ll$ stat	$\ll$ stat	$\ll$ stat	$\ll$ stat	$\ll$ stat	$\ll$ stat
Total		0.009	0.009	0.009	0.007	0.007	0.007

Table 1: Systematic uncertainties on $v_2^{\text{ch jet}}$ for various transverse momenta and centralities. Uncertainties in central and semi-central collisions are given in the same p_T ranges. The definitions of shape uncertainty and correlated uncertainty are explained in Sec. 2.5. Fields with the value '$\ll$ stat' indicate that no systematic effect can be resolved within the statistical limits of the analysis.

measured spectrum for which the singular value is small and which amplify statistical noise in the result. To explore the sensitivity of the result to the regularization strength, the effective rank of the matrix equation that is solved is varied by changing an integer regularization parameter k by $\pm$ 1. The SVD unfolding algorithm uses a prior spectrum as the starting point of the unfolding; the result of the unfolding is the ratio between the full spectrum and this prior. The unfolded solution from the χ^2 algorithm [53] is used as prior (default) as well as a PYTHIA spectrum. The bias from the choice of unfolding algorithm itself is tested by comparing the results of the SVD unfolding and the χ^2 algorithm.

The same nominal unfolding approach is used for the in-plane and out-of-plane jet spectra and the δp_T distributions for the in-plane and out-of-plane background fluctuations are similar in width; the unfolding uncertainty is therefore strongly correlated between the in-plane and out-of-plane jet spectra. These correlations are taken into account by applying the variations in the unfolding procedure to the in-plane and out-of-plane jet spectra at the same time and calculating the resulting variations of $v_2^{\text{ch jet}}$. The total uncertainty from unfolding is determined by constructing a distribution of all unfolded solutions in each p_T^{chjet} interval and assigning the width of this distribution as a systematic uncertainty.

The other two components of the shape uncertainty are the sensitivity of the unfolded solution to combinatorial jets and uncertainties arising from the description of the underlying event; both are estimated on the in-plane and out-of-plane jet spectra independently and propagated to $v_2^{\text{ch jet}}$ as uncorrelated. A systematic uncertainty is only assigned when the observed variation is found to be statistically incompatible with the nominal measurement. The effect of combinatorial jets is tested by varying the minimum p_T^{chjet} of the measured jet spectrum by $\pm$ 5 GeV/c, effectively increasing or decreasing the possible contribution of combinatorial jet yield at low jet momentum. To test the assumptions made in the fitting of Eq. 5 the maximum p_T of accepted tracks is lowered to 4 GeV/c. Additionally, the minimum p-value that is used as a goodness of fit criterion is changed from 0.01 (the nominal value) to 0.1. The minimum required distance of tracks to the leading jet axis in pseudorapidity is enlarged to 0.3.

Table 1 gives an overview of the systematic uncertainties in terms of absolute uncertainties on $v_2^{\text{ch jet}}$ for all sources (where the total uncertainty is the quadratic sum of the separate components). High statistics Monte Carlo testing has been used to verify that uncertainties labeled '$\ll$ stat' are indeed negligible compared to other uncertainties.
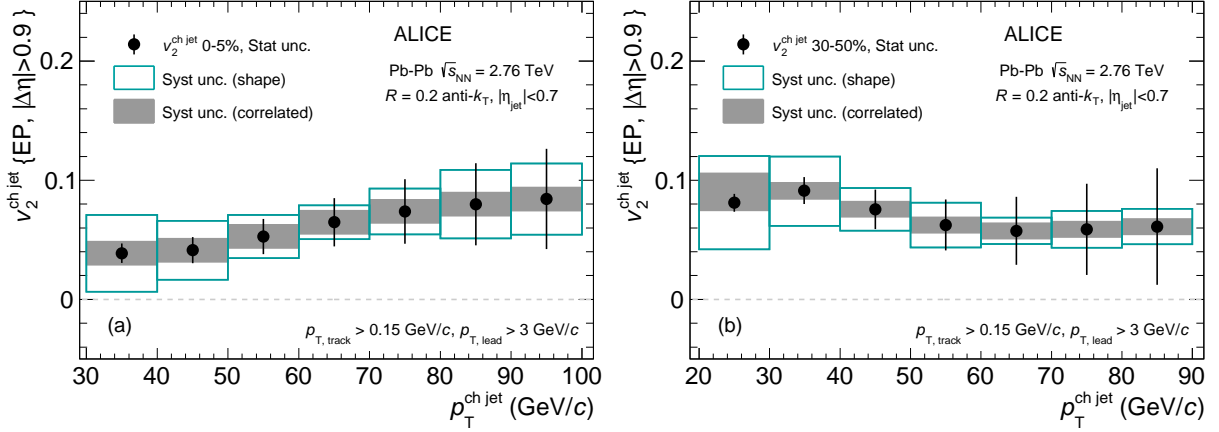
Fig. 4: Second-order harmonic coefficient $v_2^{\text{ch jet}}$ as function a of p_T^{chjet} for 0–5% (a) and 30–50% (b) collision centrality. The error bars on the points represent statistical uncertainties, the open and shaded boxes indicate the shape and correlated uncertainties (as explained in Sec. 2.5).

3   Results and discussion

The coefficients $v_2^{\text{ch jet}}$ as function of p_T^{chjet} for 0–5% and 30–50% collision centrality are presented in Fig. 4. Significant positive $v_2^{\text{ch jet}}$ is observed in semi-central collisions and no (significant) p_T dependence is visible. The observed behavior is indicative of path-length-dependent in-medium parton energy loss. The observed $v_2^{\text{ch jet}}$ in central collisions is of similar magnitude. The systematic uncertainties on the measurement however are larger than those on the semi-central $v_2^{\text{ch jet}}$ data, in particular at lower p_T^{chjet}, as a result of the larger relative background contribution to the measured jet energy.

The significance of the results is assessed by calculating a p-value for the hypothesis that $v_2^{\text{ch jet}} = 0$ over the presented momentum range. The p-value is evaluated starting from a modified χ^2 calculation that takes into account both statistical and (correlated) systematic uncertainties, as suggested in [57]. The modified χ^2 for the hypothesis $v_2^{\text{ch jet}} = \mu_i$ is calculated by minimizing

$$\tilde{\chi}^2(\varepsilon_{\text{corr}}, \varepsilon_{\text{shape}}) = \left[\left(\sum_{i=1}^{n} \frac{(v_{2,i} + \varepsilon_{\text{corr}}\sigma_{\text{corr,i}} + \varepsilon_{\text{shape}} - \mu_i)^2}{\sigma_i^2} \right) + \varepsilon_{\text{corr}}^2 + \frac{1}{n}\sum_{i=1}^{n} \frac{\varepsilon_{\text{shape}}^2}{\sigma_{\text{shape,i}}^2} \right] \tag{16}$$

with respect to the systematic shifts $\varepsilon_{\text{shape}}$, $\varepsilon_{\text{corr}}$, where $v_{2,i}$ represent the measured data (n points), σ_i are statistical uncertainties and $\sigma_{\text{shape,i}}$, $\sigma_{\text{corr,i}}$ denote the two specific types of systematic uncertainties. The parameter $\varepsilon_{\text{shape}}$ is a measure of the fully correlated shifts; a shift of all data points by the correlated incertainty $\sigma_{\text{corr,i}}$ gives a total contribution to $\tilde{\chi}^2$ of one unit. The systematic shifts for the shape uncertainty are taken to be of equal size for each point, since this gives the best agreement with the $v_2^{\text{ch jet}} = 0$ hypothesis and thus provides a conservative estimate of the significance; the penalty factor is constructed such that an average shift of all data points by σ_{shape} adds one unit to $\tilde{\chi}^2$.

The p-value itself is calculated using the χ^2 distribution with $n-2$ degrees of freedom. For semi-central collisions a p-value of 0.0009 is found, indicating significant positive $v_2^{\text{ch jet}}$. It should be noted that the most significant data points are at $p_T^{\text{chjet}} < 60$ GeV/c; the results in the range $60 < p_T^{\text{chjet}} < 100$ GeV/c are compatible with $v_2^{\text{ch jet}} = 0$ (p-value 0.02). In central collisions, a p-value with respect to the hypothesis of $v_2^{\text{ch jet}} = 0$ of 0.12 is found which indicates that $v_2^{\text{ch jet}}$ is compatible with 0 within two standard deviations. Following the same approach an upper limit of $v_2^{\text{ch jet}} = 0.088$ is found within the same confidence interval.
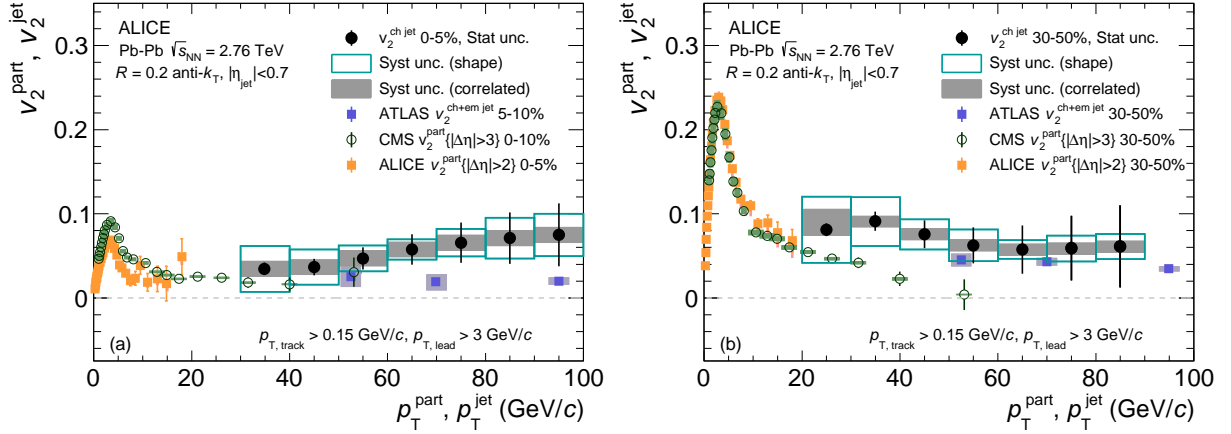
Fig. 5: Elliptic flow coefficient v_2 of charged particles [21, 22] (red, green) and $R = 0.2$ full jets (comprising both charged and neutral fragments) measured within $|\eta| < 2.1$ [58] (blue) superimposed on the results from the current analysis of $R = 0.2$ charged jets $v_2^{\text{ch jet}}$. In all measurements, statistical errors are represented by bars and systematic uncertainties by shaded or open boxes. Note that the same parton p_T corresponds to different single particle, full jet and charged jet p_T. ATLAS $v_2^{\text{ch+emjet}}$ and CMS v_2 from [22, 58] in 30–50 % centrality are the weighted arithmetic means of measurements in 10% centrality intervals using the inverse square of statistical uncertainties as weights.

3.1 Comparison to previous measurements and model predictions

To get a better qualitative understanding of the results, the v_2 of single charged particles v_2^{part} [21, 22] and the ATLAS $v_2^{\text{ch+emjet}}$ measurement [58] are shown together with the $v_2^{\text{ch jet}}$ measurement in Fig. 5. The ATLAS result is for jets with resolution parameter $R = 0.2$ within $|\eta| < 2.1$ comprising both charged and neutral fragments. The event plane angle is measured by the forward calorimeter system at $3.2 < |\eta| < 4.9$. Jets are reconstructed by applying the anti-k_T algorithm to calorimeter towers, after which, in an iterative procedure, a flow-modulated underlying event energy is subtracted. Each jet is required to lie within $\sqrt{\Delta\eta^2 + \Delta\varphi^2} < 0.2$ of either a calorimeter cluster of $p_T > 9$ GeV/c or a $p_T > 10$ GeV/c track jet with resolution parameter $R = 0.4$ built from constituent tracks of $p_T > 4$ GeV/c (the full reconstruction procedure can be found in [58, 59]).

It is important to realize that the energy scales of the ATLAS $v_2^{\text{ch+emjet}}$ and ALICE $v_2^{\text{ch jet}}$ measurements are different (as the ALICE jets do not include neutral fragments) which complicates a direct comparison between the two measurements. The central ATLAS results are also reported in 5–10% collision centrality. The ALICE and ATLAS measurements are in qualitative agreement, both indicating path-length-dependent parton energy loss. Given the uncertainties, the difference in the central values of the measurement is not significant.

Figure 5 also shows the v_2 of single charged particles v_2^{part} (from [21, 22]), which is expected to be mostly caused by in-medium energy loss at intermediate and high momenta ($p_T \gtrsim 5$ GeV/c). Even though a direct quantitative comparison between $v_2^{\text{ch jet}}$ and v_2^{part} cannot be made as the energy scales for jets and single particles are different, the measurements can be compared qualitatively, and it can be seen that for central events, the single particle v_2^{part} and $v_2^{\text{ch jet}}$ are of similar magnitude and only weakly dependent on p_T over a large range of p_T ($\approx 20 - 50$ GeV/c). For non-central collisions (30–50%), the measurements of v_2 for single particles and jets are also in qualitative agreement in the p_T range where the uncertainties allow for a comparison.

Figure 6 shows the $v_2^{\text{ch jet}}$ of $R = 0.2$ charged jets from the JEWEL Monte Carlo [29, 30] compared to the measured $v_2^{\text{ch jet}}$. JEWEL simulates a parton shower evolution in the presence of a dense QCD medium by generating hard scatterings according to a collision geometry from a Glauber [60] density profile. A 1D Bjorken expansion is used to simulate the time evolution of the medium. After radiative and collisional
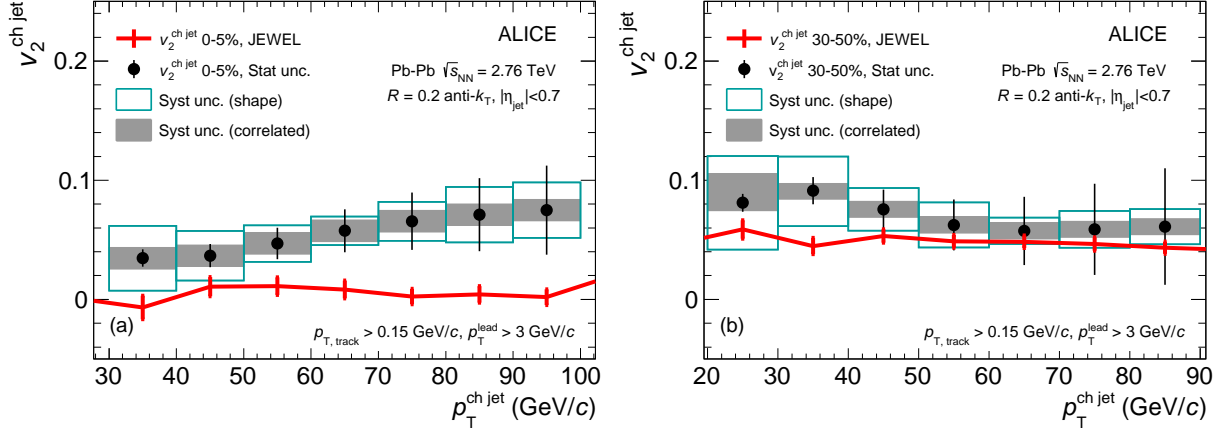
Fig. 6: $v_2^{\text{ch jet}}$ of $R = 0.2$ charged jets obtained from the JEWEL Monte Carlo (red) for central (a) and semi-central collisions (b) compared to data. JEWEL data points are presented with only statistical uncertainties.

energy loss, PYTHIA is used to hadronize the fragments to final state particles.

The analysis on the JEWEL events is performed with the same jet definition and acceptance criteria that are used for the $v_2^{\text{ch jet}}$ analysis in data, using the symmetry plane Ψ_2 from the simulated initial geometry as $\Psi_{\text{EP, 2}}$. The JEWEL Monte Carlo shows finite significant $v_2^{\text{ch jet}}$ in semi-central collisions; in central collisions $v_2^{\text{ch jet}}$ is compatible with zero. The JEWEL result for semi-central 30–50% collisions is compatible with the measured values (p-value 0.4 using Eq. 16 with the JEWEL results as hypothesis μ_i and the quadratic sum of the statistical uncertainties of both datasets as σ_i in the denominator of the first sum of Eq. 16). In central JEWEL collisions $v_2^{\text{ch jet}}$ is consistent with zero, while the measured values are compatible with the JEWEL $v_2^{\text{ch jet}}$ within two standard deviations. It should also be noted that JEWEL currently uses an optical Glauber model for the initial state and therefore does not include fluctuations in the participant distribution due to the spatial configuration of nuclei in the nucleus. This simplified treatment of the overlap geometry may underestimate the $v_2^{\text{ch jet}}$ [36, 61]. This comparison of $v_2^{\text{ch jet}}$ in JEWEL to experimental data complements earlier studies of the path-length-dependent parton energy loss and model predictions for the jet R_{AA} [5].

4   Conclusion

The azimuthal anisotropy of $R = 0.2$ charged jet production, quantified as $v_2^{\text{ch jet}}$, has been presented in central and semi-central collisions. Significant positive $v_2^{\text{ch jet}}$ is observed in semi-central collisions, which indicates that jet suppression is sensitive to the initial geometry of the overlap region of the collision. This observation can be used to constrain predictions on the path-length dependence of in-medium parton energy loss. In central collisions, the central values of the measurement are positive, but the uncertainties preclude drawing a strong conclusion on the magnitude of $v_2^{\text{ch jet}}$.

The measured $v_2^{\text{ch jet}}$ for charged jets is also compared to single particle v_2 from ALICE and CMS and $v_2^{\text{ch+emjet}}$ from ATLAS. The measurements cannot be directly compared quantitatively since the energy scales are different, but qualitatively, the results agree and indicate a positive v_2 for both charged particles and jets to high p_{T} in central and semi-central collisions. This observation indicates that parton energy loss is large and that the sensitivity to the collision geometry persists up to high transverse momenta.

The JEWEL Monte Carlo predicts sizable $v_2^{\text{ch jet}}$ for semi-central collisions and very small to zero $v_2^{\text{ch jet}}$ in central events. These predictions are in good agreement with the semi-central measurement. For central collisions, the JEWEL prediction is below the measurement, but more data would be needed to reduce the uncertainties on the measurement sufficiently to constrain the model.

Acknowledgements

References

[1] S. Bass, M. Gyulassy, H. Stoecker, and W. Greiner, "Signatures of quark gluon plasma formation in high-energy heavy ion collisions: A Critical review," *J. Phys.* **G25** (1999) R1–R57, arXiv:hep-ph/9810281 [hep-ph].

[2] R. Baier, Y. Dokshitzer, S. Peigné, and D. Schiff, "Induced gluon radiation in a QCD medium,"

Physics Letters B **345** no. 3, (1995) 277 – 286.
`http://www.sciencedirect.com/science/article/pii/037026939401617L`.

[3] M. Gyulassy and M. Plumer, "Jet Quenching in Dense Matter," *Phys. Lett.* **B243** (1990) 432–438.

[4] **ALICE** Collaboration, B. Abelev *et al.*, "Measurement of charged jet suppression in Pb-Pb collisions at $\sqrt{s_{NN}} = 2.76$ TeV," *JHEP* **1403** (2014) 013, `arXiv:1311.0633 [nucl-ex]`.

[5] **ALICE** Collaboration, J. Adam *et al.*, "Measurement of jet suppression in central Pb–Pb collisions at $\sqrt{s_{NN}} = 2.76$ TeV," *Phys. Lett.* **B746** (2015) 1–14, `arXiv:1502.01689 [nucl-ex]`.

[6] **STAR** Collaboration, J. Adams *et al.*, "Experimental and theoretical challenges in the search for the quark gluon plasma: The STAR Collaboration's critical assessment of the evidence from RHIC collisions," *Nucl. Phys.* **A757** (2005) 102–183, `arXiv:nucl-ex/0501009 [nucl-ex]`.

[7] **PHENIX** Collaboration, K. Adcox *et al.*, "Formation of dense partonic matter in relativistic nucleus-nucleus collisions at RHIC: Experimental evaluation by the PHENIX collaboration," *Nucl. Phys.* **A757** (2005) 184–283, `arXiv:nucl-ex/0410003 [nucl-ex]`.

[8] **BRAHMS** Collaboration, I. Arsene *et al.*, "Transverse momentum spectra in Au+Au and d+Au collisions at $\sqrt{s_{NN}} = 200$ GeV and the pseudorapidity dependence of high p_T suppression," *Phys.Rev.Lett.* **91** (2003) 072305, `arXiv:nucl-ex/0307003 [nucl-ex]`.

[9] **PHOBOS** Collaboration, B. Back *et al.*, "Charged hadron transverse momentum distributions in Au + Au collisions at $\sqrt{s_{NN}} = 200$ GeV," *Phys.Lett.* **B578** (2004) 297–303, `arXiv:nucl-ex/0302015 [nucl-ex]`.

[10] **ALICE** Collaboration, K. Aamodt *et al.*, "Suppression of Charged Particle Production at Large Transverse Momentum in Central Pb–Pb Collisions at $\sqrt{s_{NN}} = 2.76$ TeV," *Phys. Lett.* **B696** (2011) 30–39, `arXiv:1012.1004 [nucl-ex]`.

[11] **ALICE** Collaboration, K. Aamodt *et al.*, "Particle-yield modification in jet-like azimuthal di-hadron correlations in Pb-Pb collisions at $\sqrt{s_{NN}} = 2.76$ TeV," *Phys. Rev. Lett.* **108** (2012) 092301, `arXiv:1110.0121 [nucl-ex]`.

[12] **ATLAS** Collaboration, G. Aad *et al.*, "Measurement of charged-particle spectra in Pb+Pb collisions at $\sqrt{s_{NN}} = 2.76$ TeV with the ATLAS detector at the LHC," `arXiv:1504.04337 [hep-ex]`.

[13] **CMS** Collaboration, S. Chatrchyan *et al.*, "Study of high p_T charged particle suppression in Pb–Pb compared to pp collisions at $\sqrt{s_{NN}} = 2.76$ TeV," *Eur.Phys.J.* **C72** (2012) 1945, `arXiv:1202.2554 [nucl-ex]`.

[14] **ATLAS** Collaboration, G. Aad *et al.*, "Observation of a Centrality-Dependent Dijet Asymmetry in Lead-Lead Collisions at $\sqrt{s_{NN}} = 2.76$ TeV with the ATLAS Detector at the LHC," *Phys. Rev. Lett.* **105** (2010) 252303, `arXiv:1011.6182 [hep-ex]`.

[15] **CMS** Collaboration, S. Chatrchyan *et al.*, "Jet momentum dependence of jet quenching in Pb–Pb collisions at $\sqrt{s_{NN}} = 2.76$ TeV," *Phys.Lett.* **B712** (2012) 176–197, `arXiv:1202.5022 [nucl-ex]`.

[16] **ATLAS** Collaboration, G. Aad *et al.*, "Measurement of the jet radius and transverse momentum dependence of inclusive jet suppression in lead-lead collisions at $\sqrt{s_{NN}} = 2.76$ TeV with the ATLAS detector," *Phys.Lett.* **B719** (2013) 220–241, `arXiv:1208.1967 [hep-ex]`.

[17] R. Baier, Y. L. Dokshitzer, A. H. Mueller, S. Peigné, and D. Schiff, "Radiative energy loss of high-energy quarks and gluons in a finite volume quark - gluon plasma," *Nucl. Phys.* **B483** (1997) 291–320, `arXiv:hep-ph/9607355 [hep-ph]`.

[18] R. Baier, Y. L. Dokshitzer, A. H. Mueller, S. Peigné, and D. Schiff, "Radiative energy loss and p(T) broadening of high-energy partons in nuclei," *Nucl. Phys.* **B484** (1997) 265–282, `arXiv:hep-ph/9608322 [hep-ph]`.

[19] F. Dominguez, C. Marquet, A. H. Mueller, B. Wu, and B.-W. Xiao, "Comparing energy loss and $p_\perp$ - broadening in perturbative QCD with strong coupling N = 4 SYM theory," *Nucl. Phys.* **A811** (2008) 197–222, `arXiv:0803.3234 [nucl-th]`.

[20] C. Marquet and T. Renk, "Jet quenching in the strongly-interacting quark-gluon plasma," *Phys. Lett.* **B685** (2010) 270–276, `arXiv:0908.0880 [hep-ph]`.

[21] **ALICE** Collaboration, B. Abelev *et al.*, "Anisotropic flow of charged hadrons, pions and (anti-)protons measured at high transverse momentum in Pb-Pb collisions at $\sqrt{s_{\mathrm{NN}}}$=2.76 TeV," *Phys. Lett.* **B719** (2013) 18–28, `arXiv:1205.5761 [nucl-ex]`.

[22] **CMS** Collaboration, S. Chatrchyan *et al.*, "Azimuthal anisotropy of charged particles at high transverse momenta in Pb–Pb collisions at $\sqrt{s_{\mathrm{NN}}} = 2.76$ TeV," *Phys. Rev. Lett.* **109** (2012) 022301, `arXiv:1204.1850 [nucl-ex]`.

[23] **STAR** Collaboration, J. Adams *et al.*, "Azimuthal anisotropy and correlations at large transverse momenta in p+p and Au+Au collisions at $\sqrt{s_{\mathrm{NN}}} = 200$ GeV," *Phys. Rev. Lett.* **93** (2004) 252301, `arXiv:nucl-ex/0407007 [nucl-ex]`.

[24] **PHENIX** Collaboration, S. S. Adler *et al.*, "A Detailed Study of high-p_{T} Neutral Pion Suppression and Azimuthal Anisotropy in Au+Au Collisions at $\sqrt{s_{\mathrm{NN}}} = 200$ GeV," *Phys. Rev.* **C76** (2007) 034904, `arXiv:nucl-ex/0611007 [nucl-ex]`.

[25] **PHENIX** Collaboration, A. Adare *et al.*, "Azimuthal anisotropy of neutral pion production in Au+Au collisions at $\sqrt{s_{\mathrm{NN}}} = 200$ GeV: Path-length dependence of jet quenching and the role of initial geometry," *Phys. Rev. Lett.* **105** (2010) 142301, `arXiv:1006.3740 [nucl-ex]`.

[26] T. Renk, H. Holopainen, U. Heinz, and C. Shen, "A Systematic comparison of jet quenching in different fluid-dynamical models," *Phys. Rev.* **C83** (2011) 014910, `arXiv:1010.1635 [hep-ph]`.

[27] **STAR** Collaboration, J. Adams *et al.*, "Direct observation of dijets in central Au+Au collisions at $\sqrt{s_{\mathrm{NN}}} = 200$ GeV," *Phys. Rev. Lett.* **97** (2006) 162301, `arXiv:nucl-ex/0604018 [nucl-ex]`.

[28] **ALICE** Collaboration, J. Adam *et al.*, "Measurement of jet quenching with semi-inclusive hadron-jet distributions in central Pb-Pb collisions at $\sqrt{s_{\mathbf{NN}}} = 2.76$ TeV," `arXiv:1506.03984 [nucl-ex]`.

[29] K. C. Zapp, F. Krauss, and U. A. Wiedemann, "A perturbative framework for jet quenching," *JHEP* **1303** (2013) 080, `arXiv:1212.1599 [hep-ph]`.

[30] K. C. Zapp, "Geometrical aspects of jet quenching in JEWEL," *Phys. Lett.* **B735** (2014) 157–163, `arXiv:1312.5536 [hep-ph]`.

[31] Z.-W. Lin, C. M. Ko, B.-A. Li, B. Zhang, and S. Pal, "Multiphase transport model for relativistic heavy ion collisions," *Phys. Rev. C* **72** (2005) 064901. `http://link.aps.org/doi/10.1103/PhysRevC.72.064901`.

[32] M.-W. Nie and G.-L. Ma, "Azimuthal anisotropies of reconstructed jets in Pb–Pb collisions at $\sqrt{s_{NN}}$ = 2.76 TeV in a multiphase transport model," *Phys. Rev. C* **90** (2014) 014907. http://link.aps.org/doi/10.1103/PhysRevC.90.014907.

[33] **ALICE** Collaboration, K. Aamodt *et al.*, "The ALICE experiment at the CERN LHC," *JINST* **3** (2008) S08002.

[34] **ALICE** Collaboration, B. Abelev *et al.*, "Performance of the ALICE Experiment at the CERN LHC," *Int. J. Mod. Phys.* **A29** (2014) 1430044, arXiv:1402.4476 [nucl-ex].

[35] **ALICE** Collaboration, B. Abelev *et al.*, "Centrality determination of Pb-Pb collisions at $\sqrt{s_{NN}}$ = 2.76 TeV with ALICE," *Phys. Rev.* **C88** no. 4, (2013) 044909, arXiv:1301.4361 [nucl-ex].

[36] J.-Y. Ollitrault, "Anisotropy as a signature of transverse collective flow," *Phys. Rev.* **D46** (1992) 229–245.

[37] S. Voloshin and Y. Zhang, "Flow study in relativistic nuclear collisions by Fourier expansion of azimuthal particle distributions," *Zeitschrift für Physik C Particles and Fields* **70** no. 4, (1996) 665–671. http://dx.doi.org/10.1007/s002880050141.

[38] A. M. Poskanzer and S. A. Voloshin, "Methods for analyzing anisotropic flow in relativistic nuclear collisions," *Phys. Rev. C* **58** (1998) 1671–1678. http://link.aps.org/doi/10.1103/PhysRevC.58.1671.

[39] **ALICE** Collaboration, E. Abbas *et al.*, "Performance of the ALICE VZERO system," *JINST* **8** (2013) P10016, arXiv:1306.3130 [nucl-ex].

[40] I. Selyuzhenkov and S. Voloshin, "Effects of nonuniform acceptance in anisotropic flow measurements," *Phys. Rev. C* **77** (2008) 034904. http://link.aps.org/doi/10.1103/PhysRevC.77.034904.

[41] M. Cacciari and G. P. Salam, "Dispelling the N^3 myth for the k_T jet-finder," *Phys. Lett.* **B641** (2006) 57–61, arXiv:hep-ph/0512210 [hep-ph].

[42] M. Cacciari, G. P. Salam, and G. Soyez, "FastJet User Manual," *Eur. Phys. J.* **C72** (2012) 1896, arXiv:1111.6097 [hep-ph].

[43] **ALICE** Collaboration, B. Abelev *et al.*, "Measurement of Event Background Fluctuations for Charged Particle Jet Reconstruction in Pb-Pb collisions at $\sqrt{s_{NN}}$ = 2.76 TeV," *JHEP* **1203** (2012) 053, arXiv:1201.2423 [hep-ex].

[44] M. Cacciari, J. Rojo, G. Salam, and G. Soyez, "Jet reconstruction in heavy ion collisions," *The European Physical Journal C* **71** no. 1, (2011) . http://dx.doi.org/10.1140/epjc/s10052-011-1539-z.

[45] **ALICE** Collaboration, K. Aamodt *et al.*, "Elliptic flow of charged particles in Pb–Pb collisions at $\sqrt{s_{NN}}$ = 2.76 TeV," *Phys. Rev. Lett.* **105** (2010) 252302, arXiv:1011.3914 [nucl-ex].

[46] S. Baker and R. D. Cousins, "Clarification of the Use of Chi Square and Likelihood Functions in Fits to Histograms," *Nucl. Instrum. Meth.* **221** (1984) 437–442.

[47] G. de Barros, B. Fenton-Olsen, P. Jacobs, and M. Płoskon, "Data-driven analysis methods for the measurement of reconstructed jets in heavy ion collisions at RHIC and LHC," *Nucl. Phys.* **A910-911** (2013) 314–318, arXiv:1208.1518 [hep-ex].

[48] V. Blobel, "An Unfolding method for high-energy physics experiments," in *Advanced statistical techniques in particle physics. Proceedings, Conference, Durham, UK, March 18-22, 2002*, pp. 258–267. 2002. `arXiv:hep-ex/0208022 [hep-ex]`. `http://www.ippp.dur.ac.uk/Workshops/02/statistics/proceedings//blobel2.pdf`.

[49] M. Schmelling, "The Method of reduced cross entropy: A General approach to unfold probability distributions," *Nucl. Instrum. Meth.* **A340** (1994) 400–412.

[50] T. Sjostrand, S. Mrenna, and P. Z. Skands, "PYTHIA 6.4 Physics and Manual," *JHEP* **05** (2006) 026, `arXiv:hep-ph/0603175 [hep-ph]`.

[51] R. Brun, F. Carminati, and S. Giani, "GEANT Detector Description and Simulation Tool," CERN-W-5013.

[52] A. Hocker and V. Kartvelishvili, "SVD approach to data unfolding," *Nucl. Instrum. Meth.* **A372** (1996) 469–481, `arXiv:hep-ph/9509307 [hep-ph]`.

[53] V. Blobel, "Unfolding methods in high-energy physics experiments," DESY-84-118. `http://cds.cern.ch/record/157405`.

[54] **E877** Collaboration, Barrette, J. *et al*, "Energy and charged particle flow in 10.8A GeV/*c* Au+Au collisions," *Phys. Rev. C* **55** (1997) 1420–1430. `http://link.aps.org/doi/10.1103/PhysRevC.55.1420`.

[55] **E877** Collaboration, Barrette, J. *et al*, "Erratum: Energy and charged particle flow in 10.8A GeV/*c* Au+Au collisions [Phys. Rev. C **55**, 1420 (1997)]," *Phys. Rev. C* **56** (Oct, 1997) 2336–2336. `http://link.aps.org/doi/10.1103/PhysRevC.56.2336`.

[56] X.-N. Wang and M. Gyulassy, "HIJING: A Monte Carlo model for multiple jet production in p p, p A and A A collisions," *Phys. Rev.* **D44** (1991) 3501–3516.

[57] **PHENIX** Collaboration, A. Adare *et al.*, "Quantitative constraints on the transport properties of hot partonic matter from semi-inclusive single high transverse momentum pion suppression in Au+Au collisions at $\sqrt{s_{NN}} = 200$ GeV," *Phys. Rev. C* **77** (2008) 064907. `http://link.aps.org/doi/10.1103/PhysRevC.77.064907`.

[58] **ATLAS** Collaboration, G. Aad *et al.*, "Measurement of the Azimuthal Angle Dependence of Inclusive Jet Yields in Pb+Pb Collisions at $\sqrt{s_{NN}} = 2.76$ TeV with the ATLAS detector," *Phys. Rev. Lett.* **111** no. 15, (2013) 152301, `arXiv:1306.6469 [hep-ex]`.

[59] **ATLAS** Collaboration, G. Aad *et al.*, "Measurement of the jet radius and transverse momentum dependence of inclusive jet suppression in lead–lead collisions at $\sqrt{s_{NN}} = 2.76$ TeV with the ATLAS detector," *Phys. Lett.* **B719** (2013) 220–241, `arXiv:1208.1967 [hep-ex]`.

[60] M. L. Miller, K. Reygers, S. J. Sanders, and P. Steinberg, "Glauber modeling in high energy nuclear collisions," *Ann. Rev. Nucl. Part. Sci.* **57** (2007) 205–243, `arXiv:nucl-ex/0701025 [nucl-ex]`.

[61] **PHOBOS** Collaboration, B. Alver *et al.*, "System size, energy, pseudorapidity, and centrality dependence of elliptic flow," *Phys. Rev. Lett.* **98** (2007) 242302, `arXiv:nucl-ex/0610037 [nucl-ex]`.

A The ALICE Collaboration

J. Adam[40], D. Adamová[83], M.M. Aggarwal[87], G. Aglieri Rinella[36], M. Agnello[110], N. Agrawal[48],
Z. Ahammed[132], S.U. Ahn[68], S. Aiola[136], A. Akindinov[58], S.N. Alam[132], D. Aleksandrov[99], B. Alessandro[110],
D. Alexandre[101], R. Alfaro Molina[64], A. Alici[12 ,104], A. Alkin[3], J.R.M. Almaraz[119], J. Alme[38], T. Alt[43],
S. Altinpinar[18], I. Altsybeev[131], C. Alves Garcia Prado[120], C. Andrei[78], A. Andronic[96], V. Anguelov[93],
J. Anielski[54], T. Antičić[97], F. Antinori[107], P. Antonioli[104], L. Aphecetche[113], H. Appelshäuser[53], S. Arcelli[28],
R. Arnaldi[110], O.W. Arnold[37 ,92], I.C. Arsene[22], M. Arslandok[53], B. Audurier[113], A. Augustinus[36],
R. Averbeck[96], M.D. Azmi[19], A. Badalà[106], Y.W. Baek[67 ,44], S. Bagnasco[110], R. Bailhache[53], R. Bala[90],
A. Baldisseri[15], R.C. Baral[61], A.M. Barbano[27], R. Barbera[29], F. Barile[33], G.G. Barnaföldi[135], L.S. Barnby[101],
V. Barret[70], P. Bartalini[7], K. Barth[36], J. Bartke[117], E. Bartsch[53], M. Basile[28], N. Bastid[70], S. Basu[132],
B. Bathen[54], G. Batigne[113], A. Batista Camejo[70], B. Batyunya[66], P.C. Batzing[22], I.G. Bearden[80], H. Beck[53],
C. Bedda[110], N.K. Behera[50], I. Belikov[55], F. Bellini[28], H. Bello Martinez[2], R. Bellwied[122], R. Belmont[134],
E. Belmont-Moreno[64], V. Belyaev[75], G. Bencedi[135], S. Beole[27], I. Berceanu[78], A. Bercuci[78], Y. Berdnikov[85],
D. Berenyi[135], R.A. Bertens[57], D. Berzano[36], L. Betev[36], A. Bhasin[90], I.R. Bhat[90], A.K. Bhati[87],
B. Bhattacharjee[45], J. Bhom[128], L. Bianchi[122], N. Bianchi[72], C. Bianchin[57 ,134], J. Bielčík[40], J. Bielčíková[83],
A. Bilandzic[80], R. Biswas[4], S. Biswas[79], S. Bjelogrlic[57], J.T. Blair[118], D. Blau[99], C. Blume[53], F. Bock[93 ,74],
A. Bogdanov[75], H. Bøggild[80], L. Boldizsár[135], M. Bombara[41], J. Book[53], H. Borel[15], A. Borissov[95],
M. Borri[82 ,124], F. Bossú[65], E. Botta[27], S. Böttger[52], C. Bourjau[80], P. Braun-Munzinger[96], M. Bregant[120],
T. Breitner[52], T.A. Broker[53], T.A. Browning[94], M. Broz[40], E.J. Brucken[46], E. Bruna[110], G.E. Bruno[33],
D. Budnikov[98], H. Buesching[53], S. Bufalino[27 ,36], P. Buncic[36], O. Busch[93 ,128], Z. Buthelezi[65], J.B. Butt[16],
J.T. Buxton[20], D. Caffarri[36], X. Cai[7], H. Caines[136], L. Calero Diaz[72], A. Caliva[57], E. Calvo Villar[102],
P. Camerini[26], F. Carena[36], W. Carena[36], F. Carnesecchi[28], J. Castillo Castellanos[15], A.J. Castro[125],
E.A.R. Casula[25], C. Ceballos Sanchez[9], J. Cepila[40], P. Cerello[110], J. Cerkala[115], B. Chang[123], S. Chapeland[36],
M. Chartier[124], J.L. Charvet[15], S. Chattopadhyay[132], S. Chattopadhyay[100], V. Chelnokov[3], M. Cherney[86],
C. Cheshkov[130], B. Cheynis[130], V. Chibante Barroso[36], D.D. Chinellato[121], S. Cho[50], P. Chochula[36],
K. Choi[95], M. Chojnacki[80], S. Choudhury[132], P. Christakoglou[81], C.H. Christensen[80], P. Christiansen[34],
T. Chujo[128], S.U. Chung[95], C. Cicalo[105], L. Cifarelli[12 ,28], F. Cindolo[104], J. Cleymans[89], F. Colamaria[33],
D. Colella[59 ,33 ,36], A. Collu[74 ,25], M. Colocci[28], G. Conesa Balbastre[71], Z. Conesa del Valle[51],
M.E. Connors[ii,136], J.G. Contreras[40], T.M. Cormier[84], Y. Corrales Morales[110], I. Cortés Maldonado[2],
P. Cortese[32], M.R. Cosentino[120], F. Costa[36], P. Crochet[70], R. Cruz Albino[11], E. Cuautle[63], L. Cunqueiro[36],
T. Dahms[92 ,37], A. Dainese[107], A. Danu[62], D. Das[100], I. Das[51 ,100], S. Das[4], A. Dash[121 ,79], S. Dash[48],
S. De[120], A. De Caro[31 ,12], G. de Cataldo[103], C. de Conti[120], J. de Cuveland[43], A. De Falco[25], D. De
Gruttola[12 ,31], N. De Marco[110], S. De Pasquale[31], A. Deisting[96 ,93], A. Deloff[77], E. Dénes[135 ,i], C. Deplano[81],
P. Dhankher[48], D. Di Bari[33], A. Di Mauro[36], P. Di Nezza[72], M.A. Diaz Corchero[10], T. Dietel[89],
P. Dillenseger[53], R. Divià[36], Ø. Djuvsland[18], A. Dobrin[57 ,81], D. Domenicis Gimenez[120], B. Dönigus[53],
O. Dordic[22], T. Drozhzhova[53], A.K. Dubey[132], A. Dubla[57], L. Ducroux[130], P. Dupieux[70], R.J. Ehlers[136],
D. Elia[103], H. Engel[52], E. Epple[136], B. Erazmus[113], I. Erdemir[53], F. Erhardt[129], B. Espagnon[51],
M. Estienne[113], S. Esumi[128], J. Eum[95], D. Evans[101], S. Evdokimov[111], G. Eyyubova[40], L. Fabbietti[92 ,37],
D. Fabris[107], J. Faivre[71], A. Fantoni[72], M. Fasel[74], L. Feldkamp[54], A. Feliciello[110], G. Feofilov[131],
J. Ferencei[83], A. Fernández Téllez[2], E.G. Ferreiro[17], A. Ferretti[27], A. Festanti[30], V.J.G. Feuillard[15 ,70],
J. Figiel[117], M.A.S. Figueredo[124 ,120], S. Filchagin[98], D. Finogeev[56], F.M. Fionda[25], E.M. Fiore[33],
M.G. Fleck[93], M. Floris[36], S. Foertsch[65], P. Foka[96], S. Fokin[99], E. Fragiacomo[109], A. Francescon[30 ,36],
U. Frankenfeld[96], U. Fuchs[36], C. Furget[71], A. Furs[56], M. Fusco Girard[31], J.J. Gaardhøje[80], M. Gagliardi[27],
A.M. Gago[102], M. Gallio[27], D.R. Gangadharan[74], P. Ganoti[36 ,88], C. Gao[7], C. Garabatos[96], E. Garcia-Solis[13],
C. Gargiulo[36], P. Gasik[37 ,92], E.F. Gauger[118], M. Germain[113], A. Gheata[36], M. Gheata[62 ,36], P. Ghosh[132],
S.K. Ghosh[4], P. Gianotti[72], P. Giubellino[36], P. Giubilato[30], E. Gladysz-Dziadus[117], P. Glässel[93], D.M. Goméz
Coral[64], A. Gomez Ramirez[52], V. Gonzalez[10], P. González-Zamora[10], S. Gorbunov[43], L. Görlich[117],
S. Gotovac[116], V. Grabski[64], O.A. Grachov[136], L.K. Graczykowski[133], K.L. Graham[101], A. Grelli[57],
A. Grigoras[36], C. Grigoras[36], V. Grigoriev[75], A. Grigoryan[1], S. Grigoryan[66], B. Grinyov[3], N. Grion[109],
J.M. Gronefeld[96], J.F. Grosse-Oetringhaus[36], J.-Y. Grossiord[130], R. Grosso[96], F. Guber[56], R. Guernane[71],
B. Guerzoni[28], K. Gulbrandsen[80], T. Gunji[127], A. Gupta[90], R. Gupta[90], R. Haake[54], Ø. Haaland[18],
C. Hadjidakis[51], M. Haiduc[62], H. Hamagaki[127], G. Hamar[135], J.W. Harris[136], A. Harton[13],
D. Hatzifotiadou[104], S. Hayashi[127], S.T. Heckel[53], M. Heide[54], H. Helstrup[38], A. Herghelegiu[78], G. Herrera
Corral[11], B.A. Hess[35], K.F. Hetland[38], H. Hillemanns[36], B. Hippolyte[55], R. Hosokawa[128], P. Hristov[36],
M. Huang[18], T.J. Humanic[20], N. Hussain[45], T. Hussain[19], D. Hutter[43], D.S. Hwang[21], R. Ilkaev[98],
M. Inaba[128], M. Ippolitov[75 ,99], M. Irfan[19], M. Ivanov[96], V. Ivanov[85], V. Izucheev[111], P.M. Jacobs[74],

M.B. Jadhav[48], S. Jadlovska[115], J. Jadlovsky[115,59], C. Jahnke[120], M.J. Jakubowska[133], H.J. Jang[68], M.A. Janik[133], P.H.S.Y. Jayarathna[122], C. Jena[30], S. Jena[122], R.T. Jimenez Bustamante[96], P.G. Jones[101], H. Jung[44], A. Jusko[101], P. Kalinak[59], A. Kalweit[36], J. Kamin[53], J.H. Kang[137], V. Kaplin[75], S. Kar[132], A. Karasu Uysal[69], O. Karavichev[56], T. Karavicheva[56], L. Karayan[93,96], E. Karpechev[56], U. Kebschull[52], R. Keidel[138], D.L.D. Keijdener[57], M. Keil[36], M. Mohisin Khan[19], P. Khan[100], S.A. Khan[132], A. Khanzadeev[85], Y. Kharlov[111], B. Kileng[38], D.W. Kim[44], D.J. Kim[123], D. Kim[137], H. Kim[137], J.S. Kim[44], M. Kim[44], M. Kim[137], S. Kim[21], T. Kim[137], S. Kirsch[43], I. Kisel[43], S. Kiselev[58], A. Kisiel[133], G. Kiss[135], J.L. Klay[6], C. Klein[53], J. Klein[36,93], C. Klein-Bösing[54], S. Klewin[93], A. Kluge[36], M.L. Knichel[93], A.G. Knospe[118], T. Kobayashi[128], C. Kobdaj[114], M. Kofarago[36], T. Kollegger[96,43], A. Kolojvari[131], V. Kondratiev[131], N. Kondratyeva[75], E. Kondratyuk[111], A. Konevskikh[56], M. Kopcik[115], M. Kour[90], C. Kouzinopoulos[36], O. Kovalenko[77], V. Kovalenko[131], M. Kowalski[117], G. Koyithatta Meethaleveedu[48], I. Králik[59], A. Kravčáková[41], M. Kretz[43], M. Krivda[101,59], F. Krizek[83], E. Kryshen[36], M. Krzewicki[43], A.M. Kubera[20], V. Kučera[83], C. Kuhn[55], P.G. Kuijer[81], A. Kumar[90], J. Kumar[48], L. Kumar[87], S. Kumar[48], P. Kurashvili[77], A. Kurepin[56], A.B. Kurepin[56], A. Kuryakin[98], M.J. Kweon[50], Y. Kwon[137], S.L. La Pointe[110], P. La Rocca[29], P. Ladron de Guevara[11], C. Lagana Fernandes[120], I. Lakomov[36], R. Langoy[42], C. Lara[52], A. Lardeux[15], A. Lattuca[27], E. Laudi[36], R. Lea[26], L. Leardini[93], G.R. Lee[101], S. Lee[137], F. Lehas[81], R.C. Lemmon[82], V. Lenti[103], E. Leogrande[57], I. León Monzón[119], H. León Vargas[64], M. Leoncino[27], P. Lévai[135], S. Li[70,7], X. Li[14], J. Lien[42], R. Lietava[101], S. Lindal[22], V. Lindenstruth[43], C. Lippmann[96], M.A. Lisa[20], H.M. Ljunggren[34], D.F. Lodato[57], P.I. Loenne[18], V. Loginov[75], C. Loizides[74], X. Lopez[70], E. López Torres[9], A. Lowe[135], P. Luettig[53], M. Lunardon[30], G. Luparello[26], A. Maevskaya[56], M. Mager[36], S. Mahajan[90], S.M. Mahmood[22], A. Maire[55], R.D. Majka[136], M. Malaev[85], I. Maldonado Cervantes[63], L. Malinina[iii,66], D. Mal'Kevich[58], P. Malzacher[96], A. Mamonov[98], V. Manko[99], F. Manso[70], V. Manzari[36,103], M. Marchisone[27,65,126], J. Mareš[60], G.V. Margagliotti[26], A. Margotti[104], J. Margutti[57], A. Marín[96], C. Markert[118], M. Marquard[53], N.A. Martin[96], J. Martin Blanco[113], P. Martinengo[36], M.I. Martínez[2], G. Martínez García[113], M. Martinez Pedreira[36], A. Mas[120], S. Masciocchi[96], M. Masera[27], A. Masoni[105], L. Massacrier[113], A. Mastroserio[33], A. Matyja[117], C. Mayer[117], J. Mazer[125], M.A. Mazzoni[108], D. Mcdonald[122], F. Meddi[24], Y. Melikyan[75], A. Menchaca-Rocha[64], E. Meninno[31], J. Mercado Pérez[93], M. Meres[39], Y. Miake[128], M.M. Mieskolainen[46], K. Mikhaylov[66,58], L. Milano[36], J. Milosevic[22], L.M. Minervini[103,23], A. Mischke[57], A.N. Mishra[49], D. Miśkowiec[96], J. Mitra[132], C.M. Mitu[62], N. Mohammadi[57], B. Mohanty[79,132], L. Molnar[55,113], L. Montaño Zetina[11], E. Montes[10], D.A. Moreira De Godoy[54,113], L.A.P. Moreno[2], S. Moretto[30], A. Morreale[113], A. Morsch[36], V. Muccifora[72], E. Mudnic[116], D. Mühlheim[54], S. Muhuri[132], M. Mukherjee[132], J.D. Mulligan[136], M.G. Munhoz[120], R.H. Munzer[92,37], S. Murray[65], L. Musa[36], J. Musinsky[59], B. Naik[48], R. Nair[77], B.K. Nandi[48], R. Nania[104], E. Nappi[103], M.U. Naru[16], H. Natal da Luz[120], C. Nattrass[125], K. Nayak[79], T.K. Nayak[132], S. Nazarenko[98], A. Nedosekin[58], L. Nellen[63], F. Ng[122], M. Nicassio[96], M. Niculescu[62], J. Niedziela[36], B.S. Nielsen[80], S. Nikolaev[99], S. Nikulin[99], V. Nikulin[85], F. Noferini[12,104], P. Nomokonov[66], G. Nooren[57], J.C.C. Noris[2], J. Norman[124], A. Nyanin[99], J. Nystrand[18], H. Oeschler[93], S. Oh[136], S.K. Oh[67], A. Ohlson[36], A. Okatan[69], T. Okubo[47], L. Olah[135], J. Oleniacz[133], A.C. Oliveira Da Silva[120], M.H. Oliver[136], J. Onderwaater[96], C. Oppedisano[110], R. Orava[46], A. Ortiz Velasquez[63], A. Oskarsson[34], J. Otwinowski[117], K. Oyama[93,76], M. Ozdemir[53], Y. Pachmayer[93], P. Pagano[31], G. Paić[63], S.K. Pal[132], J. Pan[134], A.K. Pandey[48], P. Papcun[115], V. Papikyan[1], G.S. Pappalardo[106], P. Pareek[49], W.J. Park[96], S. Parmar[87], A. Passfeld[54], V. Paticchio[103], R.N. Patra[132], B. Paul[100], T. Peitzmann[57], H. Pereira Da Costa[15], E. Pereira De Oliveira Filho[120], D. Peresunko[99,75], C.E. Pérez Lara[81], E. Perez Lezama[53], V. Peskov[53], Y. Pestov[5], V. Petráček[40], V. Petrov[111], M. Petrovici[78], C. Petta[29], S. Piano[109], M. Pikna[39], P. Pillot[113], O. Pinazza[104,36], L. Pinsky[122], D.B. Piyarathna[122], M. Płoskoń[74], M. Planinic[129], J. Pluta[133], S. Pochybova[135], P.L.M. Podesta-Lerma[119], M.G. Poghosyan[84,86], B. Polichtchouk[111], N. Poljak[129], W. Poonsawat[114], A. Pop[78], S. Porteboeuf-Houssais[70], J. Porter[74], J. Pospisil[83], S.K. Prasad[4], R. Preghenella[36,104], F. Prino[110], C.A. Pruneau[134], I. Pshenichnov[56], M. Puccio[27], G. Puddu[25], P. Pujahari[134], V. Punin[98], J. Putschke[134], H. Qvigstad[22], A. Rachevski[109], S. Raha[4], S. Rajput[90], J. Rak[123], A. Rakotozafindrabe[15], L. Ramello[32], F. Rami[55], R. Raniwala[91], S. Raniwala[91], S.S. Räsänen[46], B.T. Rascanu[53], D. Rathee[87], K.F. Read[125,84], K. Redlich[77], R.J. Reed[134], A. Rehman[18], P. Reichelt[53], F. Reidt[93,36], X. Ren[7], R. Renfordt[53], A.R. Reolon[72], A. Reshetin[56], J.-P. Revol[12], K. Reygers[93], V. Riabov[85], R.A. Ricci[73], T. Richert[34], M. Richter[22], P. Riedler[36], W. Riegler[36], F. Riggi[29], C. Ristea[62], E. Rocco[57], M. Rodríguez Cahuantzi[2,11], A. Rodriguez Manso[81], K. Røed[22], E. Rogochaya[66], D. Rohr[43], D. Röhrich[18], R. Romita[124], F. Ronchetti[72,36], L. Ronflette[113], P. Rosnet[70], A. Rossi[30,36], F. Roukoutakis[88], A. Roy[49], C. Roy[55], P. Roy[100], A.J. Rubio Montero[10], R. Rui[26], R. Russo[27], E. Ryabinkin[99], Y. Ryabov[85], A. Rybicki[117], S. Sadovsky[111], K. Šafařík[36], B. Sahlmuller[53], P. Sahoo[49], R. Sahoo[49], S. Sahoo[61],

P.K. Sahu[61], J. Saini[132], S. Sakai[72], M.A. Saleh[134], J. Salzwedel[20], S. Sambyal[90], V. Samsonov[85], L. Šándor[59], A. Sandoval[64], M. Sano[128], D. Sarkar[132], E. Scapparone[104], F. Scarlassara[30], C. Schiaua[78], R. Schicker[93], C. Schmidt[96], H.R. Schmidt[35], S. Schuchmann[53], J. Schukraft[36], M. Schulc[40], T. Schuster[136], Y. Schutz[113 ,36], K. Schwarz[96], K. Schweda[96], G. Scioli[28], E. Scomparin[110], R. Scott[125], M. Šefčík[41], J.E. Seger[86], Y. Sekiguchi[127], D. Sekihata[47], I. Selyuzhenkov[96], K. Senosi[65], S. Senyukov[3 ,36], E. Serradilla[10 ,64], A. Sevcenco[62], A. Shabanov[56], A. Shabetai[113], O. Shadura[3], R. Shahoyan[36], A. Shangaraev[111], A. Sharma[90], M. Sharma[90], M. Sharma[90], N. Sharma[125], K. Shigaki[47], K. Shtejer[9 ,27], Y. Sibiriak[99], S. Siddhanta[105], K.M. Sielewicz[36], T. Siemiarczuk[77], D. Silvermyr[84 ,34], C. Silvestre[71], G. Simatovic[129], G. Simonetti[36], R. Singaraju[132], R. Singh[79], S. Singha[132 ,79], V. Singhal[132], B.C. Sinha[132], T. Sinha[100], B. Sitar[39], M. Sitta[32], T.B. Skaali[22], M. Slupecki[123], N. Smirnov[136], R.J.M. Snellings[57], T.W. Snellman[123], C. Søgaard[34], J. Song[95], M. Song[137], Z. Song[7], F. Soramel[30], S. Sorensen[125], F. Sozzi[96], M. Spacek[40], E. Spiriti[72], I. Sputowska[117], M. Spyropoulou-Stassinaki[88], J. Stachel[93], I. Stan[62], G. Stefanek[77], E. Stenlund[34], G. Steyn[65], J.H. Stiller[93], D. Stocco[113], P. Strmen[39], A.A.P. Suaide[120], T. Sugitate[47], C. Suire[51], M. Suleymanov[16], M. Suljic[26 ,i], R. Sultanov[58], M. Šumbera[83], A. Szabo[39], A. Szanto de Toledo[120 ,i], I. Szarka[39], A. Szczepankiewicz[36], M. Szymanski[133], U. Tabassam[16], J. Takahashi[121], G.J. Tambave[18], N. Tanaka[128], M.A. Tangaro[33], M. Tarhini[51], M. Tariq[19], M.G. Tarzila[78], A. Tauro[36], G. Tejeda Muñoz[2], A. Telesca[36], K. Terasaki[127], C. Terrevoli[30], B. Teyssier[130], J. Thäder[74], D. Thomas[118], R. Tieulent[130], A.R. Timmins[122], A. Toia[53], S. Trogolo[27], G. Trombetta[33], V. Trubnikov[3], W.H. Trzaska[123], T. Tsuji[127], A. Tumkin[98], R. Turrisi[107], T.S. Tveter[22], K. Ullaland[18], A. Uras[130], G.L. Usai[25], A. Utrobicic[129], M. Vajzer[83], M. Vala[59], L. Valencia Palomo[70], S. Vallero[27], J. Van Der Maarel[57], J.W. Van Hoorne[36], M. van Leeuwen[57], T. Vanat[83], P. Vande Vyvre[36], D. Varga[135], A. Vargas[2], M. Vargyas[123], R. Varma[48], M. Vasileiou[88], A. Vasiliev[99], A. Vauthier[71], V. Vechernin[131], A.M. Veen[57], M. Veldhoen[57], A. Velure[18], M. Venaruzzo[73], E. Vercellin[27], S. Vergara Limón[2], R. Vernet[8], M. Verweij[134], L. Vickovic[116], G. Viesti[30 ,i], J. Viinikainen[123], Z. Vilakazi[126], O. Villalobos Baillie[101], A. Villatoro Tello[2], A. Vinogradov[99], L. Vinogradov[131], Y. Vinogradov[98 ,i], T. Virgili[31], V. Vislavicius[34], Y.P. Viyogi[132], A. Vodopyanov[66], M.A. Völkl[93], K. Voloshin[58], S.A. Voloshin[134], G. Volpe[135], B. von Haller[36], I. Vorobyev[37 ,92], D. Vranic[96 ,36], J. Vrláková[41], B. Vulpescu[70], A. Vyushin[98], B. Wagner[18], J. Wagner[96], H. Wang[57], M. Wang[7 ,113], D. Watanabe[128], Y. Watanabe[127], M. Weber[112 ,36], S.G. Weber[96], D.F. Weiser[93], J.P. Wessels[54], U. Westerhoff[54], A.M. Whitehead[89], J. Wiechula[35], J. Wikne[22], M. Wilde[54], G. Wilk[77], J. Wilkinson[93], M.C.S. Williams[104], B. Windelband[93], M. Winn[93], C.G. Yaldo[134], H. Yang[57], P. Yang[7], S. Yano[47], C. Yasar[69], Z. Yin[7], H. Yokoyama[128], I.-K. Yoo[95], J.H. Yoon[50], V. Yurchenko[3], I. Yushmanov[99], A. Zaborowska[133], V. Zaccolo[80], A. Zaman[16], C. Zampolli[104], H.J.C. Zanoli[120], S. Zaporozhets[66], N. Zardoshti[101], A. Zarochentsev[131], P. Závada[60], N. Zaviyalov[98], H. Zbroszczyk[133], I.S. Zgura[62], M. Zhalov[85], H. Zhang[18], X. Zhang[74], Y. Zhang[7], C. Zhang[57], Z. Zhang[7], C. Zhao[22], N. Zhigareva[58], D. Zhou[7], Y. Zhou[80], Z. Zhou[18], H. Zhu[18], J. Zhu[113 ,7], A. Zichichi[28 ,12], A. Zimmermann[93], M.B. Zimmermann[54 ,36], G. Zinovjev[3], M. Zyzak[43]

Affiliation notes

[i] Deceased

[ii] Also at: Georgia State University, Atlanta, Georgia, United States

[iii] Also at: M.V. Lomonosov Moscow State University, D.V. Skobeltsyn Institute of Nuclear, Physics, Moscow, Russia

Collaboration Institutes

[1] A.I. Alikhanyan National Science Laboratory (Yerevan Physics Institute) Foundation, Yerevan, Armenia

[2] Benemérita Universidad Autónoma de Puebla, Puebla, Mexico

[3] Bogolyubov Institute for Theoretical Physics, Kiev, Ukraine

[4] Bose Institute, Department of Physics and Centre for Astroparticle Physics and Space Science (CAPSS), Kolkata, India

[5] Budker Institute for Nuclear Physics, Novosibirsk, Russia

[6] California Polytechnic State University, San Luis Obispo, California, United States

[7] Central China Normal University, Wuhan, China

[8] Centre de Calcul de l'IN2P3, Villeurbanne, France

[9] Centro de Aplicaciones Tecnológicas y Desarrollo Nuclear (CEADEN), Havana, Cuba

[10] Centro de Investigaciones Energéticas Medioambientales y Tecnológicas (CIEMAT), Madrid, Spain

[11] Centro de Investigación y de Estudios Avanzados (CINVESTAV), Mexico City and Mérida, Mexico

[12] Centro Fermi - Museo Storico della Fisica e Centro Studi e Ricerche "Enrico Fermi", Rome, Italy

[13] Chicago State University, Chicago, Illinois, USA

[14] China Institute of Atomic Energy, Beijing, China

[15] Commissariat à l'Energie Atomique, IRFU, Saclay, France

[16] COMSATS Institute of Information Technology (CIIT), Islamabad, Pakistan

[17] Departamento de Física de Partículas and IGFAE, Universidad de Santiago de Compostela, Santiago de Compostela, Spain

[18] Department of Physics and Technology, University of Bergen, Bergen, Norway

[19] Department of Physics, Aligarh Muslim University, Aligarh, India

[20] Department of Physics, Ohio State University, Columbus, Ohio, United States

[21] Department of Physics, Sejong University, Seoul, South Korea

[22] Department of Physics, University of Oslo, Oslo, Norway

[23] Dipartimento di Elettrotecnica ed Elettronica del Politecnico, Bari, Italy

[24] Dipartimento di Fisica dell'Università 'La Sapienza' and Sezione INFN Rome, Italy

[25] Dipartimento di Fisica dell'Università and Sezione INFN, Cagliari, Italy

[26] Dipartimento di Fisica dell'Università and Sezione INFN, Trieste, Italy

[27] Dipartimento di Fisica dell'Università and Sezione INFN, Turin, Italy

[28] Dipartimento di Fisica e Astronomia dell'Università and Sezione INFN, Bologna, Italy

[29] Dipartimento di Fisica e Astronomia dell'Università and Sezione INFN, Catania, Italy

[30] Dipartimento di Fisica e Astronomia dell'Università and Sezione INFN, Padova, Italy

[31] Dipartimento di Fisica 'E.R. Caianiello' dell'Università and Gruppo Collegato INFN, Salerno, Italy

[32] Dipartimento di Scienze e Innovazione Tecnologica dell'Università del Piemonte Orientale and Gruppo Collegato INFN, Alessandria, Italy

[33] Dipartimento Interateneo di Fisica 'M. Merlin' and Sezione INFN, Bari, Italy

[34] Division of Experimental High Energy Physics, University of Lund, Lund, Sweden

[35] Eberhard Karls Universität Tübingen, Tübingen, Germany

[36] European Organization for Nuclear Research (CERN), Geneva, Switzerland

[37] Excellence Cluster Universe, Technische Universität München, Munich, Germany

[38] Faculty of Engineering, Bergen University College, Bergen, Norway

[39] Faculty of Mathematics, Physics and Informatics, Comenius University, Bratislava, Slovakia

[40] Faculty of Nuclear Sciences and Physical Engineering, Czech Technical University in Prague, Prague, Czech Republic

[41] Faculty of Science, P.J. Šafárik University, Košice, Slovakia

[42] Faculty of Technology, Buskerud and Vestfold University College, Vestfold, Norway

[43] Frankfurt Institute for Advanced Studies, Johann Wolfgang Goethe-Universität Frankfurt, Frankfurt, Germany

[44] Gangneung-Wonju National University, Gangneung, South Korea

[45] Gauhati University, Department of Physics, Guwahati, India

[46] Helsinki Institute of Physics (HIP), Helsinki, Finland

[47] Hiroshima University, Hiroshima, Japan

[48] Indian Institute of Technology Bombay (IIT), Mumbai, India

[49] Indian Institute of Technology Indore, Indore (IITI), India

[50] Inha University, Incheon, South Korea

[51] Institut de Physique Nucléaire d'Orsay (IPNO), Université Paris-Sud, CNRS-IN2P3, Orsay, France

[52] Institut für Informatik, Johann Wolfgang Goethe-Universität Frankfurt, Frankfurt, Germany

[53] Institut für Kernphysik, Johann Wolfgang Goethe-Universität Frankfurt, Frankfurt, Germany

[54] Institut für Kernphysik, Westfälische Wilhelms-Universität Münster, Münster, Germany

[55] Institut Pluridisciplinaire Hubert Curien (IPHC), Université de Strasbourg, CNRS-IN2P3, Strasbourg, France

[56] Institute for Nuclear Research, Academy of Sciences, Moscow, Russia

[57] Institute for Subatomic Physics of Utrecht University, Utrecht, Netherlands

[58] Institute for Theoretical and Experimental Physics, Moscow, Russia

[59] Institute of Experimental Physics, Slovak Academy of Sciences, Košice, Slovakia

[60] Institute of Physics, Academy of Sciences of the Czech Republic, Prague, Czech Republic

[61] Institute of Physics, Bhubaneswar, India

[62] Institute of Space Science (ISS), Bucharest, Romania

[63] Instituto de Ciencias Nucleares, Universidad Nacional Autónoma de México, Mexico City, Mexico
[64] Instituto de Física, Universidad Nacional Autónoma de México, Mexico City, Mexico
[65] iThemba LABS, National Research Foundation, Somerset West, South Africa
[66] Joint Institute for Nuclear Research (JINR), Dubna, Russia
[67] Konkuk University, Seoul, South Korea
[68] Korea Institute of Science and Technology Information, Daejeon, South Korea
[69] KTO Karatay University, Konya, Turkey
[70] Laboratoire de Physique Corpusculaire (LPC), Clermont Université, Université Blaise Pascal, CNRS–IN2P3, Clermont-Ferrand, France
[71] Laboratoire de Physique Subatomique et de Cosmologie, Université Grenoble-Alpes, CNRS-IN2P3, Grenoble, France
[72] Laboratori Nazionali di Frascati, INFN, Frascati, Italy
[73] Laboratori Nazionali di Legnaro, INFN, Legnaro, Italy
[74] Lawrence Berkeley National Laboratory, Berkeley, California, United States
[75] Moscow Engineering Physics Institute, Moscow, Russia
[76] Nagasaki Institute of Applied Science, Nagasaki, Japan
[77] National Centre for Nuclear Studies, Warsaw, Poland
[78] National Institute for Physics and Nuclear Engineering, Bucharest, Romania
[79] National Institute of Science Education and Research, Bhubaneswar, India
[80] Niels Bohr Institute, University of Copenhagen, Copenhagen, Denmark
[81] Nikhef, Nationaal instituut voor subatomaire fysica, Amsterdam, Netherlands
[82] Nuclear Physics Group, STFC Daresbury Laboratory, Daresbury, United Kingdom
[83] Nuclear Physics Institute, Academy of Sciences of the Czech Republic, Řež u Prahy, Czech Republic
[84] Oak Ridge National Laboratory, Oak Ridge, Tennessee, United States
[85] Petersburg Nuclear Physics Institute, Gatchina, Russia
[86] Physics Department, Creighton University, Omaha, Nebraska, United States
[87] Physics Department, Panjab University, Chandigarh, India
[88] Physics Department, University of Athens, Athens, Greece
[89] Physics Department, University of Cape Town, Cape Town, South Africa
[90] Physics Department, University of Jammu, Jammu, India
[91] Physics Department, University of Rajasthan, Jaipur, India
[92] Physik Department, Technische Universität München, Munich, Germany
[93] Physikalisches Institut, Ruprecht-Karls-Universität Heidelberg, Heidelberg, Germany
[94] Purdue University, West Lafayette, Indiana, United States
[95] Pusan National University, Pusan, South Korea
[96] Research Division and ExtreMe Matter Institute EMMI, GSI Helmholtzzentrum für Schwerionenforschung, Darmstadt, Germany
[97] Rudjer Bošković Institute, Zagreb, Croatia
[98] Russian Federal Nuclear Center (VNIIEF), Sarov, Russia
[99] Russian Research Centre Kurchatov Institute, Moscow, Russia
[100] Saha Institute of Nuclear Physics, Kolkata, India
[101] School of Physics and Astronomy, University of Birmingham, Birmingham, United Kingdom
[102] Sección Física, Departamento de Ciencias, Pontificia Universidad Católica del Perú, Lima, Peru
[103] Sezione INFN, Bari, Italy
[104] Sezione INFN, Bologna, Italy
[105] Sezione INFN, Cagliari, Italy
[106] Sezione INFN, Catania, Italy
[107] Sezione INFN, Padova, Italy
[108] Sezione INFN, Rome, Italy
[109] Sezione INFN, Trieste, Italy
[110] Sezione INFN, Turin, Italy
[111] SSC IHEP of NRC Kurchatov institute, Protvino, Russia
[112] Stefan Meyer Institut für Subatomare Physik (SMI), Vienna, Austria
[113] SUBATECH, Ecole des Mines de Nantes, Université de Nantes, CNRS-IN2P3, Nantes, France
[114] Suranaree University of Technology, Nakhon Ratchasima, Thailand
[115] Technical University of Košice, Košice, Slovakia

[116] Technical University of Split FESB, Split, Croatia
[117] The Henryk Niewodniczanski Institute of Nuclear Physics, Polish Academy of Sciences, Cracow, Poland
[118] The University of Texas at Austin, Physics Department, Austin, Texas, USA
[119] Universidad Autónoma de Sinaloa, Culiacán, Mexico
[120] Universidade de São Paulo (USP), São Paulo, Brazil
[121] Universidade Estadual de Campinas (UNICAMP), Campinas, Brazil
[122] University of Houston, Houston, Texas, United States
[123] University of Jyväskylä, Jyväskylä, Finland
[124] University of Liverpool, Liverpool, United Kingdom
[125] University of Tennessee, Knoxville, Tennessee, United States
[126] University of the Witwatersrand, Johannesburg, South Africa
[127] University of Tokyo, Tokyo, Japan
[128] University of Tsukuba, Tsukuba, Japan
[129] University of Zagreb, Zagreb, Croatia
[130] Université de Lyon, Université Lyon 1, CNRS/IN2P3, IPN-Lyon, Villeurbanne, France
[131] V. Fock Institute for Physics, St. Petersburg State University, St. Petersburg, Russia
[132] Variable Energy Cyclotron Centre, Kolkata, India
[133] Warsaw University of Technology, Warsaw, Poland
[134] Wayne State University, Detroit, Michigan, United States
[135] Wigner Research Centre for Physics, Hungarian Academy of Sciences, Budapest, Hungary
[136] Yale University, New Haven, Connecticut, United States
[137] Yonsei University, Seoul, South Korea
[138] Zentrum für Technologietransfer und Telekommunikation (ZTT), Fachhochschule Worms, Worms, Germany